Stable difference approximations for the elastic wave equation in second order formulation

Stefan Nilsson, N. Anders Petersson, Björn Sjögreen, and Heinz-Otto Kreiss

U.S. Department of Energy

Lawrence
Livermore
National
Laboratory

June 21, 2006

DISCLAIMER

Stable difference approximations for the elastic wave equation in second order formulation*

Stefan Nilsson†, N. Anders Petersson†, Björn Sjögreen†, and Heinz-Otto Kreiss‡

June 21, 2006
Revised December 4, 2006

Abstract

We consider the three-dimensional elastic wave equation for an isotropic inhomogeneous material subject to a stress-free boundary condition. Building on our recently developed theory for difference methods for second order hyperbolic systems [Kreiss et al., SIAM J. Num. Anal. 40, 2002], we develop an explicit, second order accurate technique which is stable for all ratios of longitudinal over transverse phase velocities. The spatial discretization is self-adjoint and the stability is obtained through an energy estimate. Seismic events are often modeled using singular source terms and we device a technique to place sources independently of the grid while retaining second order accuracy away from the source. Several numerical examples are given.

1 Introduction

As a model for seismic wave propagation, we consider the elastic wave equation for an isotropic inhomogeneous material in a three-dimensional domain Ω,

$$\rho\frac{\partial^2\mathbf{u}}{\partial t^2} = \nabla\cdot\mathfrak{T} + \mathbf{f}, \quad \mathbf{x}\in\Omega,\ t\geq 0, \tag{1}$$
$$\mathfrak{T} = \lambda(\nabla\cdot\mathbf{u})\mathbf{I} + \mu\left(\nabla\mathbf{u} + \nabla\mathbf{u}^T\right),$$

subject to initial data
$$\mathbf{u}(\mathbf{x},0) = \mathbf{U}_0(\mathbf{x}), \quad \mathbf{u}_t(\mathbf{x},0) = \mathbf{U}_1(\mathbf{x}), \quad \mathbf{x}\in\Omega.$$

Here $\mathfrak{T}$ is the stress tensor, $\mathbf{u} = \mathbf{u}(\mathbf{x},t)$ is the displacement vector with Cartesian components $\mathbf{u} = (u,v,w)^T$, where $\mathbf{x} = (x,y,z)^T$ is the location and t is time. $\mathbf{f}$ is the external (volume) forcing and the material properties are characterized by the density $\rho(\mathbf{x}) > 0$, and the Lamé parameters $\lambda(\mathbf{x}) > 0$ and $\mu(\mathbf{x}) \geq 0$. The degenerate case $\mu = 0$ corresponds to acoustic wave propagation and will not be discussed here. We henceforth assume $\mu(\mathbf{x}) > 0$.

Common boundary conditions include a Dirichlet condition for $\mathbf{u}$ or a normal stress condition

$$\mathfrak{T}\cdot\hat{\mathbf{n}} = \lambda(\nabla\cdot\mathbf{u})\hat{\mathbf{n}} + \mu(\nabla\mathbf{u} + \nabla\mathbf{u}^T)\cdot\hat{\mathbf{n}} = \mathbf{g}, \tag{2}$$

which prescribes the stresses on a boundary with unit normal $\hat{\mathbf{n}}$. When $\mathbf{g} = \mathbf{0}$, this boundary condition is often called a free surface or stress-free condition. The system (1) admits longitudinal (P, or primary) and transverse (S, or secondary) waves which propagate at phase velocities

$$c_p = \sqrt{(2\mu + \lambda)/\rho}, \quad \text{and} \quad c_s = \sqrt{\mu/\rho},$$

respectively. There can also be surface waves, which travel along a free surface, as well as waves which travel along internal material discontinuities.

Finite difference approximations of the elastodynamic equations in second order formulation have been around for a long time [1]. Early methods, based on explicit centered difference approximations, were initially very successful but suffered from instability problems when a free surface boundary condition was imposed, and the ratio between the P- and S-wave velocities,

$$\nu = \frac{c_p}{c_s}$$

became too large [11] (note that $\nu > \sqrt{2}$). Ilan [12] proposed a remedy which only applied to materials with constant properties normal to the boundary, and an implicit boundary update technique was suggested by Vidale and Clayton [23]. However, no generally applicable, stable, explicit discretization was found for the second order formulation which worked for high values of ν. Due to the instability problems, alternative formulations were explored where the elastic wave equation was rewritten as a larger first order system for the three velocity and six stress components, and discretized on a staggered grid [19]. Most current finite difference methods for seismic wave propagation are based on the staggered grid technique. It is however difficult to handle complex geometry (e.g., topography) with these staggered grid methods, so there has been recent interest in more expensive methods based on unstructured meshes, such as the spectral element technique described by Komatisch and Tromp [13].

In this paper we revisit the problem of devising an explicit finite difference method for the elastic wave equation in second order formulation. Building on our recently developed theory for difference methods for second order hyperbolic systems [16], we develop a technique which is stable for all ratios c_p/c_s. We focus on the long-wave approximation where topography is neglected and the stress-free boundary condition is enforced on a flat surface which is aligned with a grid direction. However, our longer term goal is to extend the embedded boundary technique [17, 15, 14] to the elastic wave equation for handling general domains. In seismic applications, the material parameters ρ, μ, and λ often vary on a length scale which is significantly smaller than the wave length of the elastic waves. Hence the material parameters can vary rapidly on the computational grid, and to guarentee stability it is desirable to develop a numerical method which satisfies an energy estimate. For a hyperbolic system in second order formulation, the key to an energy estimate is a spatial discretization which is self-adjoint, i.e., corresponds to a symmetric or symmetrizable matrix. In this paper, we present a discretization which makes the spatial approximation second order accurate, self-adjoint, and explicit. The self-adjoint property also implies that the method is conservative.

In Section 1.1 we introduce the basic ideas behind our spatial discretization by studying the scalar wave equation with a cross term in two space dimensions. The discretization technique is generalized to the elastic wave equation in Section 2, where we present a theory proving that the method is second order accurate and stable for all values of c_p/c_s. The stability and accuracy of the new method are also illustrated with computational experiments. Seismic events (for example, earthquakes) are often modeled using singular source terms applied at points, along lines, or over surfaces in the three-dimensional domain. In Section 3 we device a technique to place sources independently of the grid while retaining second order accuracy away from the source. We also study how the temporal smoothness of a point source effects the spatial smoothness of the solution. In Section 4 we first study how the phase velocity of surface waves depends on the number of grid points per wave length. Thereafter, we solve a benchmark problem for a simplified earthquake where the sources are distributed along a plane. Some comments on our implementation of non-reflecting boundary conditions for truncating unbounded domains are also given.

2

1.1 A model problem

We introduce our discretization technique on the half-plane problem for the scalar wave equation with a cross term in 2-D,

$$\frac{\partial^2 u}{\partial t^2} = \nabla \cdot \mathbf{F}, \quad x \ge 0,\ 0 \le y \le 2\pi,\ t \ge 0, \tag{3}$$

$$\mathbf{F} = \begin{pmatrix} u_x + \alpha u_y \\ u_y + \alpha u_x \end{pmatrix},$$

with 2π-periodic solutions in the y-direction, subject to the boundary condition

$$\mathbf{F} \cdot \hat{\mathbf{n}} = u_x + \alpha u_y = 0, \quad x = 0,\ 0 \le y \le 2\pi,\ t \ge 0, \quad \text{when} \quad \hat{\mathbf{n}} = (1,0)^T. \tag{4}$$

Here α is a real constant. Similar to the elastic wave equation, the problem (3)-(4) conserves an energy:

$$\|u_t\|^2 + \|u_x\|^2 + \|u_y\|^2 + 2\alpha(u_x, u_y) = \text{const.},$$

where (u, v) is the L_2 scalar product and $\|u\|^2 = (u, u)$. We have

$$\|u_x\|^2 + \|u_y\|^2 + 2\alpha(u_x, u_y) \ge (1 - |\alpha|)\left(\|u_x\|^2 + \|u_y\|^2\right) > 0, \quad |\alpha| < 1.$$

Hence the conserved quantity is a norm, and the problem (3)-(4) is well-posed, when $|\alpha| < 1$. Conversely, it can be shown that the problem becomes ill-posed for $|\alpha| > 1$.

We introduce a grid with points $x_i = (i-1)h$, $y_j = (j-1)h$, $i = 0, 1, 2, \ldots$, $j = 1, 2, \ldots, N_y$, where $h = 2\pi/(N_y - 1)$ is the grid size. We denote a two-dimensional grid function by $u_{i,j}(t) = u(x_i, y_j, t)$. The time dependence will be suppressed when the meaning is obvious. We use the usual definitions of divided difference operators,

$$D_+^x v_{i,j} = \frac{1}{h}(v_{i+1,j} - v_{i,j}), \quad D_-^x v_{i,j} = D_+^x v_{i-1,j}, \quad D_0^x = \frac{1}{2}\left(D_+^x + D_-^x\right),$$

and corresponding expressions in the y-direction.

A second order accurate centered spatial discretization of (3) is given by

$$\frac{d^2 u_{i,j}}{dt^2} = \left(D_-^x D_+^x + D_-^y D_+^y + 2\alpha D_0^x D_0^y\right) u_{i,j}, \quad i \ge 1, \quad 1 \le j \le N_y - 1. \tag{5}$$

There are several ways to discretize the boundary condition (4) to second order accuracy. As we shall see, a good choice is

$$D_0^x u_{1,j} + \alpha D_0^y \left(\frac{u_{2,j} + u_{0,j}}{2}\right) = 0, \quad 1 \le j \le N_y - 1. \tag{6}$$

After Fourier-transforming in the y-direction (with dual variable ω), using the boundary condition (6) to eliminate the ghost point values at $i = 0$, and introducing the vector notation $\hat{\mathbf{u}} = (\hat{u}_1, \hat{u}_2, \ldots)^T$, we can write the Fourier-transformed semi-discrete problem in matrix form

$$h^2 \frac{d^2 \hat{\mathbf{u}}}{dt^2} = (A + B)\hat{\mathbf{u}}, \tag{7}$$

where

$$A = \begin{pmatrix} -\left(2 + 4\sin^2 \frac{\omega h}{2}\right) & 2 & \\ 1 & -\left(2 + 4\sin^2 \frac{\omega h}{2}\right) & 1 \\ & \ddots & \ddots & \ddots \end{pmatrix}, \quad B = \imath\alpha\sin(\omega h)\begin{pmatrix} 0 & 2 & \\ -1 & 0 & 1 \\ & \ddots & \ddots & \ddots \end{pmatrix},$$

3

and $\imath = \sqrt{-1}$. We can symmetrize (7) by the diagonal scaling

$$
S = \begin{pmatrix} 1/\sqrt{2} & 0 & \\ 0 & 1 & 0 \\ & \ddots & \ddots & \ddots \end{pmatrix}, \quad \hat{\mathbf{w}} = S\hat{\mathbf{u}}, \quad h^2 \frac{d^2\hat{\mathbf{w}}}{dt^2} = (\tilde{A} + \tilde{B})\hat{\mathbf{w}}, \quad \tilde{A} + \tilde{B} = S(A + B)S^{-1},
$$

where $\tilde{A} + \tilde{B}$ is self-adjoint. As we shall see in Section 2, the semi-discrete problem is stable if $\tilde{A} + \tilde{B}$ also is negative definite. Furthermore, when $\tilde{A} + \tilde{B}$ is self-adjoint, it is straight forward to discretize time such that the fully discrete problem becomes stable and conserves a discrete energy which is a second order accurate approximation of the conserved energy in the continuous case.

Note that it is not necessary to solve a linear system to update the ghost points. Instead of (6) we can change the boundary condition to be

$$
D_0^x u_{1j} + \alpha D_0^y u_{1j} = 0, \quad 1 \le j \le N_y - 1, \tag{8}
$$

if we also modify the difference approximation on the boundary by taking the cross-term one-sided in the direction normal to the boundary,

$$
\frac{d^2 u_{1,j}}{dt^2} = \left(D_-^x D_+^x + D_-^y D_+^y + 2\alpha D_+^x D_0^y \right) u_{1,j}, \quad 1 \le j \le N_y - 1. \tag{9}
$$

After Fourier transforming (9) in the y-direction and eliminating the ghost point by use of (8), we obtain the same matrix representation as before, showing that the two formulations are equivalent.

2 The elastic wave equation

In Cartesian component form, the system (1) is

$$
\rho u_{tt} = \frac{\partial}{\partial x}\left((2\mu + \lambda)u_x + \lambda v_y + \lambda w_z\right) + \frac{\partial}{\partial y}\left(\mu v_x + \mu u_y\right) + \frac{\partial}{\partial z}\left(\mu u_z + \mu w_x\right) + f^{(x)}, \tag{10}
$$

$$
\rho v_{tt} = \frac{\partial}{\partial x}\left(\mu v_x + \mu u_y\right) + \frac{\partial}{\partial y}\left((2\mu + \lambda)v_y + \lambda u_x + \lambda w_z\right) + \frac{\partial}{\partial z}\left(\mu v_z + \mu w_y\right) + f^{(y)}, \tag{11}
$$

$$
\rho w_{tt} = \frac{\partial}{\partial x}\left(\mu u_z + \mu w_x\right) + \frac{\partial}{\partial y}\left(\mu v_z + \mu w_y\right) + \frac{\partial}{\partial z}\left((2\mu + \lambda)w_z + \lambda u_x + \lambda v_y\right) + f^{(z)}. \tag{12}
$$

In this paper, we consider box-shaped domains: $0 \le x \le a$, $0 \le y \le b$, $0 \le z \le c$ and impose a normal stress boundary condition at $z = 0$. In component form, the boundary condition (2) is

$$
\mu u_z + \mu w_x = g^{(x)}, \tag{13}
$$

$$
\mu v_z + \mu w_y = g^{(y)}, \quad z = 0, \ 0 \le x \le a, \ 0 \le y \le b, \ t \ge 0, \tag{14}
$$

$$
(2\mu + \lambda)w_z + \lambda u_x + \lambda v_y = g^{(z)}. \tag{15}
$$

For the purpose of discussing the stability properties of our method, we impose homogeneous Dirichlet conditions at $z = c$,

$$
\mathbf{u}(x, y, c, t) = 0, \quad 0 \le x \le a, \ 0 \le y \le b, \ t \ge 0, \tag{16}
$$

and periodic boundary conditions in the x- and y-directions. Note that the stability results can be extended to the case of Dirichlet conditions in the x- and y-directions.

To simplify our notation, we assume zero volume and boundary forcings ($\mathbf{f} = \mathbf{0}$ and $\mathbf{g} = \mathbf{0}$) throughout sections 2.1-2.3.

4

2.1 Spatial discretization

The conclusion from the model problem in Section 1.1 is that a stable second order accurate discretization of (3)-(4) can be obtained by discretizing the differential equation with centered differences, except for the cross-terms on the boundary which should be taken one-sided in the direction normal to the boundary. The resulting approximation will be second order accurate and the ghost points can be updated explicitly if the tangential derivatives in the boundary conditions are discretized by centered differences along the boundary. We shall use these principles to define the difference scheme for the three-dimensional elastic wave equation and proceed by verifying that the resulting approximation is stable and second order accurate. The underlying ideas are the same as for the model problem, even though the algebra gets more complicated.

We define a three-dimensional grid with points $x_i = (i-1)h$, $y_j = (j-1)h$, $z_k = (k-1)h$, $0 \le i \le N_x$, $0 \le j \le N_y$, $0 \le k \le N_z$, where $h > 0$ is the grid size and $x_{N_x} = a$, $y_{N_y} = b$, and $z_{N_z} = c$. Time is discretized with step size $\delta_t > 0$ on a grid $t_n = n\delta_t$, $n = 0, 1, \ldots$, and we denote a grid function by $u_{i,j,k}^n = u(x_i, y_j, z_k, t_n)$. The superscript for time will be surpressed when the meaning is obvious. Apart from the difference operators already defined, we also introduce

$$\widetilde{D_0^z} v_{i,j,k} = \begin{cases} D_+^z v_{i,j,1}, & k = 1, \\ D_0^z v_{i,j,k}, & k \ge 2, \end{cases}$$

and the averaging operators

$$E_{1/2}^x(\gamma_{i,j,k}) = \gamma_{i+1/2,j,k} := \frac{\gamma_{i+1,j,k} + \gamma_{i,j,k}}{2},$$

$$E_{1/2}^y(\gamma_{i,j,k}) = \gamma_{i,j+1/2,k} := \frac{\gamma_{i,j+1,k} + \gamma_{i,j,k}}{2},$$

$$E_{1/2}^z(\gamma_{i,j,k}) = \gamma_{i,j,k+1/2} := \frac{\gamma_{i,j,k+1} + \gamma_{i,j,k}}{2}.$$

We form the spatially discrete equations at the grid points $1 \le i \le N_x - 1$, $1 \le j \le N_y - 1$, $1 \le k \le N_z - 1$,

$$\rho \frac{d^2 u}{dt^2} = D_-^x \left(E_{1/2}^x (2\mu + \lambda) D_+^x u \right) + D_-^y \left(E_{1/2}^y (\mu) D_+^y u \right) + D_-^z \left(E_{1/2}^z (\mu) D_+^z u \right)$$
$$+ D_0^x \left(\lambda D_0^y v + \lambda \widetilde{D_0^z} w \right) + D_0^y (\mu D_0^x v) + \widetilde{D_0^z} (\mu D_0^x w) =: L^{(u)}(u, v, w), \tag{17}$$

$$\rho \frac{d^2 v}{dt^2} = D_-^x \left(E_{1/2}^x (\mu) D_+^x v \right) + D_-^y \left(E_{1/2}^y (2\mu + \lambda) D_+^y v \right) + D_-^z \left(E_{1/2}^z (\mu) D_+^z v \right)$$
$$+ D_0^x (\mu D_0^y u) + D_0^y \left(\lambda D_0^x u + \lambda \widetilde{D_0^z} w \right) + \widetilde{D_0^z} (\mu D_0^y w) =: L^{(v)}(u, v, w), \tag{18}$$

$$\rho \frac{d^2 w}{dt^2} = D_-^x \left(E_{1/2}^x (\mu) D_+^x w \right) + D_-^y \left(E_{1/2}^y (\mu) D_+^y w \right) + D_-^z \left(E_{1/2}^z (2\mu + \lambda) D_+^z w \right)$$
$$+ D_0^x \left(\mu \widetilde{D_0^z} u \right) + D_0^y \left(\mu \widetilde{D_0^z} v \right) + \widetilde{D_0^z} (\lambda D_0^x u + \lambda D_0^y v) =: L^{(w)}(u, v, w), \tag{19}$$

where grid point indices have been suppressed to improve readability. The free surface boundary conditions (13)-(15) are discretized by

$$\frac{1}{2} \left(\mu_{i,j,3/2} D_+^z u_{i,j,1} + \mu_{i,j,1/2} D_+^z u_{i,j,0} \right) + \mu_{i,j,1} D_0^x w_{i,j,1} = 0, \tag{20}$$

$$\frac{1}{2} \left(\mu_{i,j,3/2} D_+^z v_{i,j,1} + \mu_{i,j,1/2} D_+^z v_{i,j,0} \right) + \mu_{i,j,1} D_0^y w_{i,j,1} = 0, \tag{21}$$

$$\frac{1}{2} \left((2\mu + \lambda)_{i,j,3/2} D_+^z w_{i,j,1} + (2\mu + \lambda)_{i,j,1/2} D_+^z w_{i,j,0} \right) + \lambda_{i,j,1} \left(D_0^x u_{i,j,1} + D_0^y v_{i,j,1} \right) = 0, \tag{22}$$

for $1 \leq i \leq N_x - 1$, $1 \leq j \leq N_y - 1$. The Dirichlet boundary condition (16) is discretized by

$$\mathbf{u}_{i,j,N_z} = \mathbf{0}, \quad 1 \leq i \leq N_x, \ 1 \leq j \leq N_y. \tag{23}$$

The discrete counterpart of the periodic boundary conditions are

$$\mathbf{u}_{N_x,j,k} = \mathbf{u}_{1,j,k}, \quad \mathbf{u}_{0,j,k} = \mathbf{u}_{N_x-1,j,k}, \tag{24}$$

$$\mathbf{u}_{i,N_y,k} = \mathbf{u}_{i,1,k}, \quad \mathbf{u}_{i,0,k} = \mathbf{u}_{i,N_y-1,k}, \tag{25}$$

for $1 \leq i \leq N_x$, $1 \leq j \leq N_y$, $1 \leq k \leq N_z$.

In (17)–(19), z-derivatives in the cross terms are made one sided at the grid line $k = 1$. Nevertheless, the semi-discrete approximation is a second order accurate approximation as demonstrated in the following theorem.

Theorem 1 *The semi-discrete scheme (17)-(19) subject to the boundary conditions (20)-(25) is a second order accurate approximation of the continuous equation (10)-(12) subject to the boundary conditions (13)-(16).*

Proof: See Appendix A. □

We will show that the above scheme satisfies an energy estimate. The energy estimate relies on the spatial discretization being self-adjoint and negative definite (elliptic). These properties are stated in three lemmas below. The main stability estimate is stated after the lemmas.

The diagonal scaling S which was used to symmetrize the spatial discretization for the model problem in Section 1.1 is related to a weighted scalar product for the unscaled problem. For the three-dimensional elastic wave equation, the appropriate scalar product and norm are

$$(w, v)_h = h^2 \sum_{i=1}^{N_x-1} \sum_{j=1}^{N_y-1} \left(\frac{h}{2} w_{i,j,1} v_{i,j,1} + h \sum_{k=2}^{N_z-1} w_{i,j,k} v_{i,j,k} \right), \quad \|v\|_h^2 = (v, v)_h.$$

The self-adjoint property is expressed in

Lemma 1 *For all real-valued grid functions (u^0, v^0, w^0), (u^1, v^1, w^1) which satisfy the discrete boundary conditions (20)-(25), the spatial operator $(L^{(u)}, L^{(v)}, L^{(w)})$ is self-adjoint, i.e.,*

$$\left(u^0, L^{(u)}(u^1, v^1, w^1) \right)_h + \left(v^0, L^{(v)}(u^1, v^1, w^1) \right)_h + \left(w^0, L^{(w)}(u^1, v^1, w^1) \right)_h =$$
$$\left(u^1, L^{(u)}(u^0, v^0, w^0) \right)_h + \left(v^1, L^{(v)}(u^0, v^0, w^0) \right)_h + \left(w^1, L^{(w)}(u^0, v^0, w^0) \right)_h. \tag{26}$$

Proof: See Appendix B. □

From the self-adjoint property it follows that there exists a conserved quantity:

Lemma 2 *All real-valued solutions (u, v, w) of the semi-discrete scheme (17)-(19) subject to the boundary conditions (20)-(25), satisfy*

$$\|\rho^{1/2} u_t\|_h^2 + \|\rho^{1/2} v_t\|_h^2 + \|\rho^{1/2} w_t\|_h^2 - (u, L^{(u)}(u, v, w))_h - (v, L^{(v)}(u, v, w))_h - (w, L^{(w)}(u, v, w))_h = C, \tag{27}$$

where C is a constant which depends on the initial data.

Proof: Lemma 1 gives

$$\frac{1}{2}\frac{d}{dt}\left(\|\rho^{1/2}u_t\|_h^2 + \|\rho^{1/2}v_t\|_h^2 + \|\rho^{1/2}w_t\|_h^2\right) =$$

$$(u_t, L^{(u)}(u,v,w))_h + (v_t, L^{(v)}(u,v,w))_h + (w_t, L^{(w)}(u,v,w))_h =$$

$$\frac{1}{2}\left((u_t, L^{(u)}(u,v,w))_h + (v_t, L^{(v)}(u,v,w))_h + (w_t, L^{(w)}(u,v,w))_h\right)$$

$$+ \frac{1}{2}\left((u, L^{(u)}(u_t,v_t,w_t))_h + (v, L^{(v)}(u_t,v_t,w_t))_h + (w, L^{(w)}(u_t,v_t,w_t))_h\right) =$$

$$\frac{1}{2}\frac{d}{dt}\left((u, L^{(u)}(u,v,w))_h + (v, L^{(v)}(u,v,w))_h + (w, L^{(w)}(u,v,w))_h\right).$$

Integrating the above relation in time starting at $t = 0$ gives (27) and shows that the constant C depends on the initial data. $\square$

To prove that the semi-discrete scheme is stable we need to show that the conserved quantity in (27) is a norm, i.e., we need to show that the spatial operator is negative definite. In particular, we need to show that the sum of the mixed terms in $(u, L^{(u)})_h$, $(v, L^{(v)})_h$, and $(w, L^{(w)})_h$, (such as $\left(D_0^x w, \mu \widetilde{D_0^z} u\right)_h$), is dominated by the sum of the strictly positive terms (such as $\left(D_+^x w, E_{1/2}^x(\mu) D_+^x w\right)_h$ when $\mu > 0$). This is straight forward in the corresponding continuous case and leads to the well known formula for the elastic energy. What makes the discrete case more challenging is that all derivatives in the strictly positive terms are discretized by operators such as $D_+^x D_-^x$, while they are discretized by centered differences (such as $D_0^x D_0^y$) in all mixed terms. We have

Lemma 3 *For all real valued grid functions (u,v,w) which satisfy the boundary conditions (20)-(25), we have*

$$(u, L^{(u)}(u,v,w))_h + (v, L^{(v)}(u,v,w))_h + (w, L^{(w)}(u,v,w))_h = -2\|(E_{1/2}^x(\mu))^{1/2}D_+^x u\|_h^2$$

$$- 2\|(E_{1/2}^y(\mu))^{1/2}D_+^y v\|_h^2 - 2\|(E_{1/2}^z(\mu))^{1/2}D_+^z w\|_h^2 - \|\lambda^{1/2}(D_0^x u + D_0^y v + \widetilde{D_0^z}w)\|_h^2$$

$$- \|\mu^{1/2}(D_0^x u + D_0^y v)\|_h^2 - \|\mu^{1/2}(\widetilde{D_0^z}v + D_0^y w)\|_h^2 - \|\mu^{1/2}(\widetilde{D_0^z}u + D_0^x w)\|_h^2 - \frac{h^2}{4}R - B. \quad (28)$$

The operator $\left(L^{(u)}, L^{(v)}, L^{(w)}\right)$ is negative definite when $\mu > 0$ and $\lambda > 0$. It is semi-definite when $\mu = 0$ and $\lambda > 0$. The remainder term R and the boundary term B are both positive. They are given by

$$R = \|\lambda^{1/2}D_+^x D_-^x u\|_h^2 + \|\mu^{1/2}D_+^y D_-^y u\|_h^2 + \|\mu^{1/2}D_+^z D_-^z u\|_{hr}^2$$

$$+ \|\mu^{1/2}D_+^x D_-^x v\|_h^2 + \|\lambda^{1/2}D_+^y D_-^y v\|_h^2 + \|\mu^{1/2}D_+^z D_-^z v\|_{hr}^2$$

$$+ \|\mu^{1/2}D_+^x D_-^x w\|_h^2 + \|\mu^{1/2}D_+^y D_-^y w\|_h^2 + \|\lambda^{1/2}D_+^z D_-^z w\|_{hr}^2. \quad (29)$$

and

$$B = h\sum_{j=1}^{N_y}\sum_{i=1}^{N_x}\left(\frac{\lambda_{i,j,N_z}}{2}w_{i,j,N_z-1}^2 + \frac{\mu_{i,j,N_z}}{2}(u_{i,j,N_z-1}^2 + v_{i,j,N_z-1}^2) + h^2\mu_{i,j,3/2}(D_+^z w_{i,j,1})^2\right). \quad (30)$$

Note: The reduced scalar product $(u,v)_{hr}$ is similar to the standard scalar product, except that it starts the summation from $k = 2$,

$$(w,v)_{hr} = h^3\sum_{i=1}^{N_x-1}\sum_{j=1}^{N_y-1}\sum_{k=2}^{N_z-1} w_{i,j,k}v_{i,j,k}, \quad \|v\|_{hr}^2 = (v,v)_{hr}.$$

Proof: The identity (28) is derived in Appendix C. All terms on the right hand side of (28) are non-positive when the functions μ and λ are non-negative. Therefore the operator is at least negative semi-definite. Negative definiteness is proved by showing that

$$(u, L^{(u)}(u, v, w))_h + (v, L^{(v)}(u, v, w))_h + (w, L^{(w)}(u, v, w))_h = 0 \tag{31}$$

implies $u_{i,j,k} = 0$, $v_{i,j,k} = 0$, and $w_{i,j,k} = 0$ at all grid points.

Assume that $\mu_{i,j,k} > 0$ and $\lambda_{i,j,k} > 0$ for all i, j, k, and that (31) holds. The right hand side of (28) is a sum of non-positive terms. Therefore, each term must be zero to make the sum zero. Hence the third scalar product term on the right hand side of (28) gives that

$$D_+^z w_{i,j,k} = 0, \quad 1 \le i \le N_x - 1, \ 1 \le j \le N_y - 1, \ 1 \le k \le N_z - 1.$$

Together with the boundary condition $w_{i,j,N_z} = 0$, this gives

$$0 = w_{i,j,N_z} = w_{i,j,N_z-1} = \ldots = w_{i,j,1}$$

Thus $w_{i,j,k} = 0$ everywhere, except possibly at $k = 0$. Next we show that $u_{i,j,k} = 0$ for all i, j, k except possibly for $k = 0$. The seventh scalar product term on the right hand side of (28) gives

$$\widetilde{D_0^z} u_{i,j,k} + D_0^x w_{i,j,k} = 0, \quad 1 \le i \le N_x - 1, \ 1 \le j \le N_y - 1, \ 1 \le k \le N_z - 1. \tag{32}$$

Because $w_{i,j,k} = 0$, (32) gives

$$u_{i,j,N_z} = u_{i,j,N_z-2} = u_{i,j,N_z-4} = \ldots \tag{33}$$

$$u_{i,j,N_z-1} = u_{i,j,N_z-3} = u_{i,j,N_z-5} = \ldots . \tag{34}$$

The boundary term B contains u_{i,j,N_z-1}^2 which therefore must be zero. Hence, (33) and (34) together with the boundary condition $u_{i,j,N_z} = 0$, give

$$0 = u_{i,j,N_z} = u_{i,j,N_z-1} = \ldots = u_{i,j,1}.$$

We have shown that $u_{i,j,k} = 0$ for all i, j, k except possibly for $k = 0$. The property $v_{i,j,k} = 0$, except possibly for $k = 0$, follows in exactly the same way as for $u_{i,j,k}$ by studying the sixth term on the right hand side of (28). The possibilities $u_{i,j,0} \ne 0$, $v_{i,j,0} \ne 0$, or $w_{i,j,0} \ne 0$ remain. However, when (u, v, w) is zero for $1 \le k \le N_z$, the boundary conditions (20)–(22) give that $u_{i,j,0} = v_{i,j,0} = w_{i,j,0} = 0$. We have now proved that the operator $(L^{(u)}, L^{(v)}, L^{(w)})$ is negative definite when μ and λ are positive functions.

If $\mu = 0$ and $\lambda > 0$, the operator has a non-trivial null-space. Take for example $u_{i,j,k} = f_{j,k}$, $v_{i,j,k} = g_{i,k}$, and $w_{i,j,k} = 0$ with $f_{j,k}, g_{i,k}$ satisfying $f_{j,N_z} = g_{i,N_z} = 0$ and periodic in the j- and i-directions respectively, but otherwise arbitrary. Because $\mu = 0$, these functions satisfy the free surface boundary conditions (20)–(22). It is an easy exercise to show that these functions make (28) equal to zero when $\mu = 0$ everywhere. Hence the operator $(L^{(u)}, L^{(v)}, L^{(w)})$ is negative semi-definite when $\mu = 0$ and $\lambda > 0$. □

The findings in Lemmas 1–3 are summarized in the following main theorem, showing that the semi-discrete problem is well-posed.

Theorem 2 *The solution of the semi-discrete scheme (17)-(19) subject to the boundary conditions (20)-(25) satisfies*

$$\|\rho^{1/2} u_t\|_h^2 + \|\rho^{1/2} v_t\|_h^2 + \|\rho^{1/2} w_t\|_h^2 - (u, L^{(u)}(u, v, w))_h - (v, L^{(v)}(u, v, w))_h - (w, L^{(w)}(u, v, w))_h = C,$$

where C is a constant that depends on the initial data. The quantity

$$-(u, L^{(u)}(u, v, w))_h - (v, L^{(v)}(u, v, w))_h - (w, L^{(w)}(u, v, w))_h$$

is positive definite when $\mu > 0$ and $\lambda > 0$, and is therefore a norm.

8

2.2 Fully discrete equations

Following the theory in [16], we discretize (17)-(19) in time according to

$$\rho\left(\frac{u^{n+1} - 2u^n + u^{n-1}}{\delta_t^2}\right) = L^{(u)}(u^n, v^n, w^n), \tag{35}$$

$$\rho\left(\frac{v^{n+1} - 2v^n + v^{n-1}}{\delta_t^2}\right) = L^{(v)}(u^n, v^n, w^n), \tag{36}$$

$$\rho\left(\frac{w^{n+1} - 2w^n + w^{n-1}}{\delta_t^2}\right) = L^{(w)}(u^n, v^n, w^n). \tag{37}$$

To simplify the notation, we introduce the weighted ρ-norm

$$(w,v)_\rho = h^2 \sum_{i=1}^{N_x-1} \sum_{j=1}^{N_y-1} \left(\frac{h}{2}\rho_{i,j,1}w_{i,j,1}v_{i,j,1} + h\sum_{k=2}^{N_z-1}\rho_{i,j,k}w_{i,j,k}v_{i,j,k}\right), \quad \|v\|_\rho^2 = (v,v)_\rho.$$

Trivial calculations give

$$\left(w, \rho^{-1}v\right)_\rho = (w,v)_h. \tag{38}$$

To show that the fully discrete scheme is energy conserving, we consider the quantity

$$\begin{aligned}
C_e(t_{n+1}) &= \left\|D_+^t u^n\right\|_\rho^2 + \left\|D_+^t v^n\right\|_\rho^2 + \left\|D_+^t w^n\right\|_\rho^2 - \left(u^{n+1}, \rho^{-1}L^{(u)}(u^n, v^n, w^n)\right)_\rho \\
&\quad - \left(v^{n+1}, \rho^{-1}L^{(v)}(u^n, v^n, w^n)\right)_\rho - \left(w^{n+1}, \rho^{-1}L^{(w)}(u^n, v^n, w^n)\right)_\rho \\
&= \left\|D_+^t u^n\right\|_\rho^2 + \left\|D_+^t v^n\right\|_\rho^2 + \left\|D_+^t w^n\right\|_\rho^2 \\
&\quad - \left(u^{n+1}, D_+^t D_-^t u^n\right)_\rho - \left(v^{n+1}, D_+^t D_-^t v^n\right)_\rho - \left(w^{n+1}, D_+^t D_-^t w^n\right)_\rho.
\end{aligned} \tag{39}$$

We have the following energy conservation result for the difference scheme.

Theorem 3 *The solution computed by the difference scheme (35)–(37) together with the boundary conditions (20)–(25) satsifies*

$$C_e(t_{n+1}) = C_e(t_n),$$

i.e., $C_e(t_n)$ is a conserved quantity for the fully discrete scheme.

Proof: Expanding the square in the term $||D_+^t u^n||_\rho^2$ (and similarly for v and w) gives the identity,

$$\begin{aligned}
\delta_t^2 C_e(t_{n+1}) &= \|u^{n+1}\|_\rho^2 + \|u^n\|_\rho^2 - \left(u^{n+1}, 2u^n + \delta_t^2\rho^{-1}L^{(u)}(u^n, v^n, w^n)\right)_\rho + \\
&\quad \|v^{n+1}\|_\rho^2 + \|v^n\|_\rho^2 - \left(v^{n+1}, 2v^n + \delta_t^2\rho^{-1}L^{(v)}(u^n, v^n, w^n)\right)_\rho + \\
&\quad \|w^{n+1}\|_\rho^2 + \|w^n\|_\rho^2 - \left(w^{n+1}, 2w^n + \delta_t^2\rho^{-1}L^{(w)}(u^n, v^n, w^n)\right)_\rho. \tag{40}
\end{aligned}$$

We have,

$$u^{n+1} + u^{n-1} = 2u^n + \delta_t^2\rho^{-1}L^{(u)}(u^n, v^n, w^n),$$

and corresponding expressions for v and w. Hence,

$$\delta_t^2 C_e(t_{n+1}) = \|u^{n+1}\|_\rho^2 + \|u^n\|_\rho^2 - \left(u^{n+1}, u^{n+1} + u^{n-1}\right)_\rho + \|v^{n+1}\|_\rho^2 + \|v^n\|_\rho^2 -$$
$$\left(v^{n+1}, v^{n+1} + v^{n-1}\right)_\rho + \|w^{n+1}\|_\rho^2 + \|w^n\|_\rho^2 - \left(w^{n+1}, w^{n+1} + w^{n-1}\right)_\rho$$
$$= \|u^n\|_\rho^2 + \|u^{n-1}\|_\rho^2 - \left(u^{n-1}, 2u^n + \delta_t^2 \rho^{-1} L^{(u)}(u^n, v^n, w^n)\right)_\rho +$$
$$\|v^n\|_\rho^2 + \|v^{n-1}\|_\rho^2 - \left(v^{n-1}, 2v^n + \delta_t^2 \rho^{-1} L^{(v)}(u^n, v^n, w^n)\right)_\rho +$$
$$\|w^n\|_\rho^2 + \|w^{n-1}\|_\rho^2 - \left(w^{n-1}, 2w^n + \delta_t^2 \rho^{-1} L^{(w)}(u^n, v^n, w^n)\right)_\rho .$$

The relation (38) gives

$$\left(u^{n-1}, \delta_t^2 \rho^{-1} L^{(u)}(u^n, v^n, w^n)\right)_\rho = \left(u^{n-1}, \delta_t^2 L^{(u)}(u^n, v^n, w^n)\right)_h ,$$

so Lemma 1 yields

$$\left(u^{n-1}, \delta_t^2 \rho^{-1} L^{(u)}(u^n, v^n, w^n)\right)_\rho + \left(v^{n-1}, \delta_t^2 \rho^{-1} L^{(v)}(u^n, v^n, w^n)\right)_\rho +$$
$$\left(w^{n-1}, \delta_t^2 \rho^{-1} L^{(w)}(u^n, v^n, w^n)\right)_\rho =$$
$$\left(u^n, \delta_t^2 \rho^{-1} L^{(u)}(u^{n-1}, v^{n-1}, w^{n-1})\right)_\rho + \left(v^n, \delta_t^2 \rho^{-1} L^{(v)}(u^{n-1}, v^{n-1}, w^{n-1})\right)_\rho +$$
$$\left(w^n, \delta_t^2 \rho^{-1} L^{(w)}(u^{n-1}, v^{n-1}, w^{n-1})\right)_\rho . \quad (41)$$

We conclude that

$$C_e(t_{n+1}) = C_e(t_n),$$

i.e., $C_e(t_n)$ is a conserved quantity for the fully discrete scheme. $\square$

To obtain an energy estimate we need to show that $C_e > 0$. This was done in [16] for approximations of the scalar wave equation. We here perform a similar analysis for the scheme (35)–(37). To make the presentation more compact, we introduce the vector notation

$$(\mathbf{u}^{n+1}, \mathbf{L}(\mathbf{u}^n))_h =: (u^{n+1}, L^{(u)}(u^n, v^n, w^n))_h + (v^{n+1}, L^{(v)}(u^n, v^n, w^n))_h + (w^{n+1}, L^{(w)}(u^n, v^n, w^n))_h. \quad (42)$$

As we shall see below, it is natural to study the scaled eigenvalue problem

$$\rho^{-1} \mathbf{L}(\mathbf{w}) = \zeta \mathbf{w}, \quad (43)$$

where $\mathbf{w}$ satisfies the boundary conditions (20)–(25). We know from Lemma 1 that $\mathbf{L}$ is self-adjoint with respect to $(\cdot, \cdot)_h$. Therefore, $\rho^{-1} \mathbf{L}$ is self-adjoint with respect to $(\cdot, \cdot)_\rho$ because

$$(\mathbf{v}, \rho^{-1} \mathbf{L}(\mathbf{w}))_\rho = (\mathbf{v}, \mathbf{L}(\mathbf{w}))_h = (\mathbf{L}(\mathbf{v}), \mathbf{w})_h = (\rho^{-1} \mathbf{L}(\mathbf{v}), \mathbf{w})_\rho.$$

Hence, the eigenvalues of (43) are real and Lemma 3 implies that they are negative, i.e.,

$$-\max_m |\zeta_m| \|\mathbf{w}\|_\rho^2 \le (\mathbf{w}, \rho^{-1} \mathbf{L}(\mathbf{w}))_\rho \le -\min_m |\zeta_m| \|\mathbf{w}\|_\rho^2. \quad (44)$$

We have the following stability result.

Theorem 4 *If the eigenvalues ζ_m of (43) satisfy the CFL-condition*

$$\frac{\delta_t^2}{4} \max_m |\zeta_m| < 1, \tag{45}$$

then the conserved quantity $C_e(t_{n+1})$ is a norm which is bounded by

$$\frac{\min_m |\zeta_m|}{4} \|\mathbf{u}^{n+1} + \mathbf{u}^n\|_\rho^2 \leq C_e(t_{n+1}) \leq \|D_+^t \mathbf{u}^n\|_\rho^2 + \frac{\max_m |\zeta_m|}{4} \|\mathbf{u}^{n+1} + \mathbf{u}^n\|_\rho^2. \tag{46}$$

If the time-step satisfies the (slightly) stricter condition

$$\frac{\delta_t^2}{4} (\max_m |\zeta_m| + \min_m |\zeta_m|) < 1, \tag{47}$$

the solution satisfies the energy estimate

$$\|\mathbf{u}^{n+1}\|_\rho^2 + \|\mathbf{u}^n\|_\rho^2 \leq \frac{2}{\min_m |\zeta_m|} C_e(t_0). \tag{48}$$

Proof: Using the vector notation (42), we can write the conserved quantity (39) as

$$C_e(t_{n+1}) = \left\| D_+^t \mathbf{u}^n \right\|_\rho^2 - \left(\mathbf{u}^{n+1}, \mathbf{L}(\mathbf{u}^n) \right)_h.$$

Because the operator $\mathbf{L}$ is self-adjoint (Lemma 1),

$$(\mathbf{u}^{n+1}, \mathbf{L}(\mathbf{u}^n))_h = \frac{1}{2}(\mathbf{u}^{n+1}, \mathbf{L}(\mathbf{u}^n))_h + \frac{1}{2}(\mathbf{u}^n, \mathbf{L}(\mathbf{u}^{n+1}))_h.$$

Furthermore,

$$(\mathbf{u}^{n+1} + \mathbf{u}^n, \mathbf{L}(\mathbf{u}^{n+1} + \mathbf{u}^n))_h - (\mathbf{u}^{n+1} - \mathbf{u}^n, \mathbf{L}(\mathbf{u}^{n+1} - \mathbf{u}^n))_h = 2(\mathbf{u}^n, \mathbf{L}(\mathbf{u}^{n+1}))_h + 2(\mathbf{u}^{n+1}, \mathbf{L}(\mathbf{u}^n))_h,$$

and $(\mathbf{w}, \mathbf{L}(\mathbf{w}))_h = (\mathbf{w}, \rho^{-1}\mathbf{L}(\mathbf{w}))_\rho$. Hence,

$$\delta_t^2 C_e(t_{n+1}) = \|\mathbf{u}^{n+1} - \mathbf{u}^n\|_\rho^2 - \frac{\delta_t^2}{4}(\mathbf{u}^{n+1} + \mathbf{u}^n, \rho^{-1}\mathbf{L}(\mathbf{u}^{n+1} + \mathbf{u}^n))_\rho + \frac{\delta_t^2}{4}(\mathbf{u}^{n+1} - \mathbf{u}^n, \rho^{-1}\mathbf{L}(\mathbf{u}^{n+1} - \mathbf{u}^n))_\rho. \tag{49}$$

The eigenvalue bound (44) gives

$$\delta_t^2 C_e(t_{n+1}) \geq \left(1 - \frac{\delta_t^2}{4} \max_m |\zeta_m|\right) \|\mathbf{u}^{n+1} - \mathbf{u}^n\|_\rho^2 + \frac{\delta_t^2}{4} \min_m |\zeta_m| \|\mathbf{u}^{n+1} + \mathbf{u}^n\|_\rho^2, \tag{50}$$

$$\delta_t^2 C_e(t_{n+1}) \leq \left(1 - \frac{\delta_t^2}{4} \min_m |\zeta_m|\right) \|\mathbf{u}^{n+1} - \mathbf{u}^n\|_\rho^2 + \frac{\delta_t^2}{4} \max_m |\zeta_m| \|\mathbf{u}^{n+1} + \mathbf{u}^n\|_\rho^2. \tag{51}$$

Therefore, $C_e \geq \min_m |\zeta_m| \|\mathbf{u}^{n+1} + \mathbf{u}^n\|_\rho^2 / 4$ when

$$1 - \frac{\delta_t^2}{4} \max_m |\zeta_m| > 0,$$

i.e., when the CFL-condition (45) is satisfied. The estimate (51) gives the upper bound in (46).

To show (48), we use the estimate

$$\|\mathbf{u}^{n+1}\|_\rho^2 + \|\mathbf{u}^n\|_\rho^2 = \frac{1}{4}\|(\mathbf{u}^{n+1} - \mathbf{u}^n) + (\mathbf{u}^{n+1} + \mathbf{u}^n)\|_\rho^2 + \frac{1}{4}\|(\mathbf{u}^n - \mathbf{u}^{n+1}) + (\mathbf{u}^n + \mathbf{u}^{n+1})\|_\rho^2$$

$$\leq \frac{1}{2}\|\mathbf{u}^{n+1} - \mathbf{u}^n\|_\rho^2 + \frac{1}{2}\|\mathbf{u}^{n+1} + \mathbf{u}^n\|_\rho^2.$$

If the condition (47) is satisfied, we have $1 - \delta_t^2 \max_m |\zeta_m|/4 > \delta_t^2 \min_m |\zeta_m|/4$, so (50) gives

$$C_e(t_{n+1}) \geq \frac{1}{4} \min_m |\zeta_m| \left(\|\mathbf{u}^{n+1} - \mathbf{u}^n\|_\rho^2 + \|\mathbf{u}^{n+1} + \mathbf{u}^n\|_\rho^2\right) \geq \frac{1}{2} \min_m |\zeta_m| \left(\|\mathbf{u}^{n+1}\|_\rho^2 + \|\mathbf{u}^n\|_\rho^2\right).$$

Furthermore, $C_e(t_{n+1}) = C_e(t_0)$, which proves the energy estimate (48). $\square$
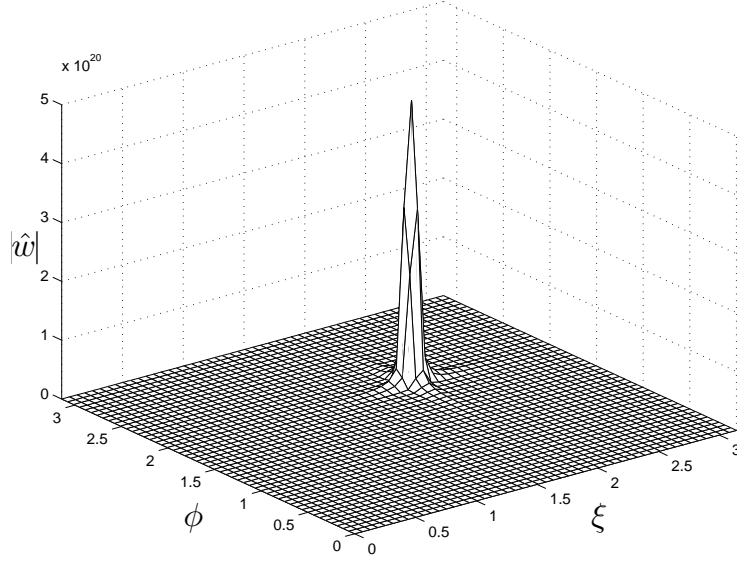
11

Figure 1: Magnitude of the two dimensional discrete Fourier transform of w at $t = 1.78$, along the $z = 0$ (stress free) surface calculated with a time step allowed by the von Neumann analysis, which underestimates the largest eigenvalue of the spatial operator. In this calculation, $\rho = 1$, $\mu = 1$, $\lambda = 79$, $h = 0.04$, $\delta_t = 0.95\delta_{tvN}$, and the initial data was given by (69). Note that all energy is concentrated around the wave numbers $\omega_x h \approx \omega_y h \approx 2\pi/3$.

2.3 Time step restrictions

In the case of constant ρ, μ, λ, and periodic boundary conditions in all three directions, a von Neumann analysis gives the maximum eigenvalue

$$\zeta_{vN} = \begin{cases} -\dfrac{4}{h^2} \dfrac{4\mu + \lambda}{\rho}, & \lambda < 2\mu, \\[3mm] -\dfrac{9}{2h^2} \dfrac{(2\mu + \lambda)^2}{\rho(\mu + \lambda)}, & \lambda \geq 2\mu. \end{cases} \tag{52}$$

If ζ_{vN} is used to estimate the largest eigenvalue $\max_m |\zeta_m|$, we get the time step restriction $\delta_t < \delta_{tvN}$, where

$$\delta_{tvN} = \begin{cases} h\sqrt{\dfrac{\rho}{4\mu + \lambda}} = \dfrac{h}{\sqrt{c_p^2 + 2c_s^2}}, & c_p < 2c_s, \\[3mm] \dfrac{\sqrt{8}h}{3} \dfrac{\sqrt{\rho(\mu + \lambda)}}{2\mu + \lambda} = \dfrac{\sqrt{8}h}{3} \dfrac{\sqrt{c_p^2 - c_s^2}}{c_p^2}, & c_p \geq 2c_s. \end{cases} \tag{53}$$

Unfortunately, numerical simulations using a time-step smaller but close to the limit (53) become unstable when a stress free boundary is imposed and the ratio $\nu = c_p/c_s$ is large, see Figure 1.

To estimate how the free-surface boundary condition modifies the time step restriction, we study the stability of the discrete half-plane problem with constant values of ρ, μ, λ. In this approximation, we assume a 2π-periodic solution in the x- and y-directions, expand the grid in the z-direction by taking $N_z \to \infty$ and replace the Dirichlet boundary condition (23) by

$$\lim_{k \to \infty} |\mathbf{u}_{i,j,k}^n| = 0. \tag{54}$$

12

Several stability definitions for difference approximations are possible and we refer to [9] for a discussion. Here we use a normal-mode approach and define the half-plane problem to be stable if there are no solutions of the form

$$\mathbf{u}(x_i, y_j, z_k, t_n) = \chi^n e^{\iota(\omega_x x_i + \omega_y y_j)} \hat{\mathbf{u}}_k, \quad \sum_{k=1}^{\infty} |\hat{\mathbf{u}}_k|^2 < \infty, \quad |\chi| > 1, \tag{55}$$

where $\iota = \sqrt{-1}$. For simplicity we assume that $N_x = N_y$ is odd. Then, $\omega_x, \omega_y = 0, \pm 1, \pm 2, \ldots, \pm(N_x - 1)/2$.

It is straight forward to perform the stability analysis if we first re-write our scheme (17)-(19) into an equivalent form, where the one-sided discretization of the cross-derivatives at $k = 1$ are replaced by the centered discretization used for $k \geq 2$, i.e., replace $\widetilde{D_0^z}$ by D_0^z in (17)-(19). We arrive at an equivalent problem by introducing compensating terms in the boundary conditions, see Appendix A. In the case of constant coefficients, the compensated stress-free boundary conditions are

$$D_0^z u_{i,j,1} + D_0^x \left(w_{i,j,1} + (\nu^2 - 1)\frac{h^2}{4} D_+^z D_-^z w_{i,j,1} \right) = 0, \tag{56}$$

$$D_0^z v_{i,j,1} + D_0^y \left(w_{i,j,1} + (\nu^2 - 1)\frac{h^2}{4} D_+^z D_-^z w_{i,j,1} \right) = 0, \tag{57}$$

$$\nu^2 D_0^z w_{i,j,1} + D_0^x \left((\nu^2 - 2)u_{i,j,1} + (\nu^2 - 1)\frac{h^2}{4} D_+^z D_-^z u_{i,j,1} \right) +$$

$$D_0^y \left((\nu^2 - 2)v_{i,j,1} + (\nu^2 - 1)\frac{h^2}{4} D_+^z D_-^z v_{i,j,1} \right) = 0. \tag{58}$$

After inserting the ansatz (55) into the modified version of (17)-(19), we arrive at the eigenvalue problem

$$\frac{\zeta_{hp}}{c_s^2} \hat{\mathbf{u}}_k := \frac{\chi - 2 + \chi^{-1}}{\delta_t^2 c_s^2} \hat{\mathbf{u}}_k = -\frac{4}{h^2} \left(\sin^2 \frac{\xi}{2} + \sin^2 \frac{\phi}{2} \right) \hat{\mathbf{u}}_k + D_+^z D_-^z \hat{\mathbf{u}}_k$$

$$+ (\nu^2 - 1) \begin{pmatrix} -\frac{4}{h^2} \sin^2 \frac{\xi}{2} & -\frac{1}{h^2} \sin \xi \sin \phi & \frac{\iota}{h} \sin \xi D_0^z \\ -\frac{1}{h^2} \sin \xi \sin \phi & -\frac{4}{h^2} \sin^2 \frac{\phi}{2} & \frac{\iota}{h} \sin \phi D_0^z \\ \frac{\iota}{h} \sin \xi D_0^z & \frac{\iota}{h} \sin \phi D_0^z & D_+^z D_-^z \end{pmatrix} \hat{\mathbf{u}}_k, \tag{59}$$

where $\xi = \omega_x h$ and $\phi = \omega_y h$ satisfy $-\pi \leq \xi \leq \pi$, $-\pi \leq \phi \leq \pi$. Inserting the ansatz (55) into the boundary conditions (56)-(58) gives

$$D_0^z \hat{u}_1 + \frac{\iota}{h} \sin \xi \left(\hat{w}_1 + (\nu^2 - 1)\frac{h^2}{4} D_+^z D_-^z \hat{w}_1 \right) = 0, \tag{60}$$

$$D_0^z \hat{v}_1 + \frac{\iota}{h} \sin \phi \left(\hat{w}_1 + (\nu^2 - 1)\frac{h^2}{4} D_+^z D_-^z \hat{w}_1 \right) = 0, \tag{61}$$

$$\nu^2 D_0^z \hat{w}_1 + \frac{\iota}{h} \sin \xi \left((\nu^2 - 2)\hat{u}_1 + (\nu^2 - 1)\frac{h^2}{4} D_+^z D_-^z \hat{u}_1 \right)$$

$$+ \frac{\iota}{h} \sin \phi \left((\nu^2 - 2)\hat{v}_1 + (\nu^2 - 1)\frac{h^2}{4} D_+^z D_-^z \hat{v}_1 \right) = 0. \tag{62}$$

The eigenvalue problem (59) can be solved using the ansatz

$$\hat{\mathbf{u}}_k = \mathbf{U} \kappa^k, \quad \text{where } |\kappa| < 1. \tag{63}$$

13

Lemma 1 is straight forward to generalize to the half-plane problem, so the spatial operator is self-adjoint, and the generalization of Lemma 3 shows that the spatial operator is negative semi-definite. All eigenvalues ζ_{hp} are therefore real and non-positive.

Next we study the relation between ζ_{hp} and χ in (59). The roots of the quadratic equation $\chi^2 - (2 - |\zeta_{hp}|\delta_t^2)\chi + 1 = 0$ are given by

$$\chi_{1,2} = 1 - \frac{|\zeta_{hp}|\delta_t^2}{2} \pm \sqrt{\Delta}, \quad \Delta = -|\zeta_{hp}|\delta_t^2\left(1 - \frac{|\zeta_{hp}|\delta_t^2}{4}\right).$$

If $\Delta < 0$, the roots are complex conjugates. Since the product of the roots equals one, both roots satisfy $|\chi_{1,2}| = 1$. If $\Delta = 0$, $\chi_{1,2} = -1$ is a double root. Finally, if $\Delta > 0$, both roots are real. One root will have magnitude greater than one and one less than one. Hence, the condition $|\chi| > 1$ in the normal mode ansatz (55) is equivalent to $\Delta > 0$. Conversely, there are no solutions of the form (55) if all eigenvalues ζ_{hp} satisfy

$$-|\zeta_{hp}|\delta_t^2\left(1 - \frac{|\zeta_{hp}|\delta_t^2}{4}\right) \leq 0, \quad \text{i.e.,} \quad \frac{\delta_t^2}{4}|\zeta_{hp}| \leq 1.$$

Hence the normal mode stability definition leads to the same type of time step restriction as in the energy method (Theorem 4), and we can use the most negative eigenvalue ζ_{hp} to approximate the eigenvalue in (45). This approximation will lead to a more restrictive time step limitation than in the von Neumann analysis if there are any eigenvalues ζ_{hp} such that

$$|\zeta_{hp}| > |\zeta_{vN}|.$$

Inserting (63) into (59) gives

$$\begin{pmatrix} -4(\nu^2 \sin^2 \frac{\xi}{2} + \sin^2 \frac{\phi}{2}) + & & \\ \kappa - 2 + \kappa^{-1} - \tilde{\zeta} & -(\nu^2 - 1)\sin\xi \sin\phi & (\nu^2-1)\imath\sin\xi(\kappa - \kappa^{-1}) \\ & -4(\sin^2 \frac{\xi}{2} + \nu^2 \sin^2 \frac{\phi}{2}) + & \\ -(\nu^2 - 1)\sin\xi\sin\phi & \kappa - 2 + \kappa^{-1} - \tilde{\zeta} & (\nu^2-1)\imath\sin\phi(\kappa - \kappa^{-1}) \\ & & -4(\sin^2 \frac{\xi}{2} + \sin^2 \frac{\phi}{2}) + \\ (\nu^2-1)\imath\sin\xi(\kappa - \kappa^{-1}) & (\nu^2-1)\imath\sin\phi(\kappa - \kappa^{-1}) & \nu^2(\kappa - 2 + \kappa^{-1}) - \tilde{\zeta} \end{pmatrix} \mathbf{U} = 0, \quad (64)$$

where $\tilde{\zeta} = \zeta_{hp}h^2/c_s^2$. Multiply (64) by κ and let

$$P(\tilde{\zeta}, \kappa, \xi, \phi, \nu) = 0, \tag{65}$$

be the corresponding characteristic equation. Here, P is a cubic polynomial in $\tilde{\zeta}$ and a polynomial of degree six in κ. For fixed ν, ξ, and ϕ there are six roots κ for each $\tilde{\zeta}$. The following Lemma is a standard result, see e.g., [10], which we here formulate for our discretization of the elastic wave equation.

Lemma 4 *The characteristic equation $P = 0$ has six roots κ_l. For $\tilde{\zeta} < -|\tilde{\zeta}_{vN}| = -|\zeta_{vN}|h^2/c_s^2$, three of these roots have $|\kappa| < 1$ and three have $|\kappa| > 1$.*

Proof: A polynomial of degree six has six roots (counting multiplicity). If any κ is such that $|\kappa| = 1$, then $\kappa = e^{\imath\alpha}$ for some real α, and (65) becomes identical to the relation obtained in the von Neumann analysis of the fully periodic problem. We know that there are no eigenvalues with magnitude greater than $|\tilde{\zeta}_{vN}|$ in this case. Therefore there can be no κ on the unit circle when $\tilde{\zeta} < -|\tilde{\zeta}_{vN}|$. Secondly, take $\phi = \xi = 0$. It is not hard to see that the characteristic equation $P = 0$ becomes

$$\left[\kappa^2 - (2 + \tilde{\zeta})\kappa + 1\right]\left[\kappa^2 - (2 + \tilde{\zeta})\kappa + 1\right]\left[\kappa^2 - (2 + \frac{\tilde{\zeta}}{\nu^2})\kappa + 1\right] = 0.$$

14

Therefore the six roots κ satisfy the pairwise relations $\kappa_1 \kappa_4 = 1$, $\kappa_2 \kappa_5 = 1$, and $\kappa_3 \kappa_6 = 1$. Since no root can be on the unit circle when $\tilde{\zeta} < -|\tilde{\zeta}_{vN}|$, there must be three roots inside the unit circle, and three roots outside of it. Furthermore, the roots κ are smooth functions of ϕ, ξ, ν, and $\tilde{\zeta}$. Because they can not move across the unit circle when $\tilde{\zeta} < -|\tilde{\zeta}_{vN}|$, the roots are always divided into these two groups for all values of ϕ, ξ, ν, and for any $\tilde{\zeta}$ such that $\tilde{\zeta} < -|\tilde{\zeta}_{vN}|$. $\square$

It follows from Lemma 4 that the general solution of (59) subject to the boundary condition (54) is

$$\hat{\mathbf{u}}_k = C_1 \mathbf{U}_1 \kappa_1^k + C_2 \mathbf{U}_2 \kappa_2^k + C_3 \mathbf{U}_3 \kappa_3^k, \quad |\kappa_l| < 1, \quad l = 1, 2, 3. \tag{66}$$

where $\mathbf{U}_l$ are the eigenvectors corresponding to κ_l, $l = 1, 2, 3$ respectively. For each $\tilde{\zeta} < -|\tilde{\zeta}_{vN}|$, $\mathbf{U}_l$ is the null-vector of the linear system (64) when the root κ_l is substituted for κ.

Inserting the general solution (66) into the stress-free boundary conditions (60)–(62) leads to a homogeneous linear system for the coefficients C_1, C_2 and C_3:

$$A \begin{pmatrix} C_1 \\ C_2 \\ C_3 \end{pmatrix} = \mathbf{0}, \tag{67}$$

where $A = A(\tilde{\zeta}, \xi, \phi, \nu)$ is a three by three matrix. There are non-trivial solutions of (67) if and only if $\det A = 0$. If (67) has a non-trivial solution $(C_1, C_2, C_3)^T$ for some $\tilde{\zeta}$, then the corresponding ζ_{hp} is an eigenvalue of (59).

Since the algebra involved in forming $\det A$ is rather complicated, we have resolved to calculating the roots of $\det A = 0$ numerically. The determinant depends on four parameters, where $\nu = c_p/c_s$ is a material constant and the angles ξ, ϕ satisfy $-\pi \le \xi, \phi \le \pi$. For each fixed ν, we need to find the angles ξ, ϕ that give the most negative solution $\tilde{\zeta}$ of $\det A = 0$. A straight forward approach is to discretize ξ, ϕ on a fine mesh:

$$\xi_p = -\pi + p \frac{2\pi}{N_\xi}, \quad p = 0, 1, 2, \dots, N_\xi,$$

$$\phi_q = -\pi + q \frac{2\pi}{N_\phi}, \quad q = 0, 1, 2, \dots, N_\phi.$$

At each mesh point $\det A$ is a complex-valued function of the real variable $\tilde{\zeta}$ and we only need to consider $\tilde{\zeta} < -|\tilde{\zeta}_{vN}|$, since only such eigenvalues can restrict the time step beyond the von Neumann limit. At each point (ξ_p, η_q), we apply a numerical root finding routine to locate the most negative solution $\tilde{\zeta}_{p,q}$ of $\det A = 0$. We then use $\min_{p,q} \tilde{\zeta}_{p,q}$ as an approximation of the most negative solution $\tilde{\zeta}$ corresponding to ν. The fundamental operation when applying a numerical root finding routine is to evaluate $\det A$ at a given value of $\tilde{\zeta}$, which can be broken down into the following steps:

1. Solve the characteristic equation (65) for κ. Select the three roots with $|\kappa_l| < 1$;

2. Find the three eigenvectors $\mathbf{U}_l$ by solving (64) for each κ_l, $l = 1, 2, 3.$;

3. Form the matrix A by inserting (66) into (60)–(62);

4. Compute the determinant of A.

Using the numerical root finding procedure outlined above, we calculated the ratio between the largest stable time step for the half-plane problem with a stress free boundary, and the largest stable time step for the fully periodic case, see Figure 2. The numerical root finding procedure located the largest eigenvalue $|\zeta_{hp}|$ at $\phi = \xi = 2\pi/3$. Hence, the spatial frequencies $\omega_x h = \omega_y h = 2\pi/3$ should grow the fastest if the
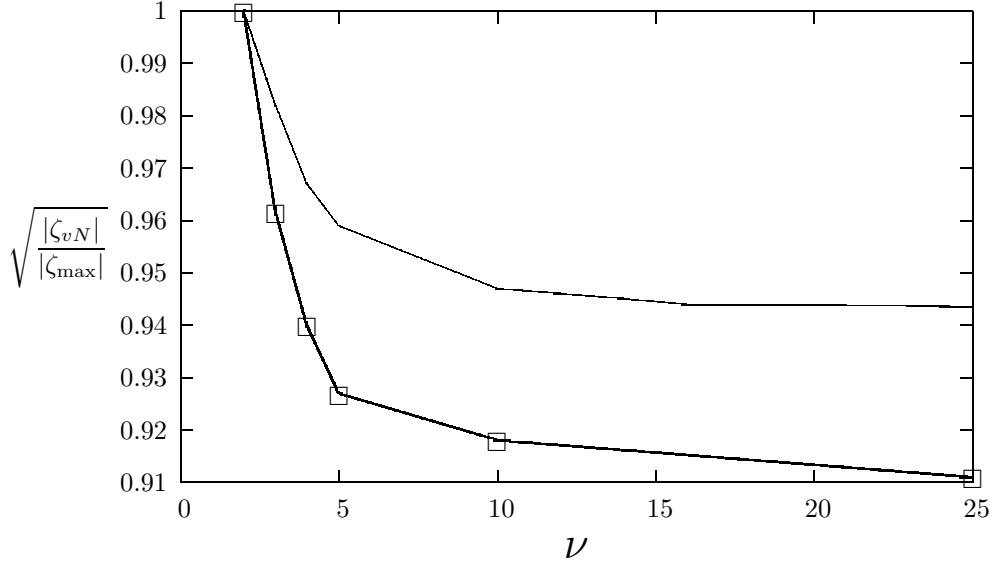
15

Figure 2: Ratio between the maximum stable time step for the half-plane problem with a free surface, and that of the fully periodic problem. The line with boxes corresponds to the three-dimensional problem and the two-dimensional case is shown with a solid line.

time-step exceeds the stability limit and ν is large. This prediction was confirmed by spatially Fourier transforming an unstable numerical solution, see Figure 1.

For large ν, the solutions of $\det A = 0$ corresponding to the largest $|\tilde{\zeta}|$ were numerically found to occur when κ_1 is real with $-1 < \kappa_1 < 0$ and $\kappa_2 = \bar{\kappa}_3$ with $-1 < \text{Re}(\kappa_{2,3}) < 0$. Thus, the eigenfunction corresponding to the largest eigenvalue oscillates in the z-direction with two different frequencies; the fastest frequency on the mesh: $|\kappa_1|^k(-1)^k$ and more slowly: $|\kappa_2|^k(\exp(\pm \iota \arg \kappa_2))^k$, where $\arg(\kappa_2) \approx 2\pi/3$ for large ν. This boundary layer behavior has been observed in numerical solutions when the time step exceeds the stability limit.

Note that the limitations imposed on the time step by the stress free boundary are very moderate even for extreme ν values (most solid materials occuring in nature have $c_p/c_s \leq 3$). As ν gets large, the largest stable time step for the half-plane problem tends to a factor exceeding 0.91 of that for the fully periodic problem. Our practical experience with the time-stepping algorithm on bounded domains with variable coefficients and a free surface boundary condition on one side indicates that it is stable when the half-plane problem with constant coefficients is stable, using the smallest time step obtained by evaluating c_p and c_s at all grid points. Hence, we can handle all values of c_p/c_s by reducing the time step by less than 9% compared to the von Neumann value. This makes our method practically useful for all isotropic materials.

The additional time-step restriction due to the free-surface boundary condition indicates that there are numerical surface waves which travel faster than any volume waves on the grid. In the continuous problem, Rayleigh (surface) waves always have a phase velocity bounded by c_s. Hence, it is likely that the numerical phase velocity for Rayleigh waves will depend on the grid resolution in terms of the number of grid points per wave length. Numerical experiments along these lines are presented in Section 4.1.

We also analyzed the two-dimensional version of the scheme by assuming that the solution does not depend on y. Here a von Neumann analysis of the doubly periodic case (ρ, μ, and λ constant) gives a

time step restriction

$$\delta_t < \frac{h\sqrt{\rho}}{\sqrt{3\mu + \lambda}} = \frac{h}{\sqrt{c_p^2 + c_s^2}}. \tag{68}$$

The stability restriction on the time step with the free surface boundary condition can be obtained using the above root finding procedure with $\phi = 0$. The results are given in Figure 2 together with the three-dimensional case. When ν becomes large, the largest stable time step for the half-plane problem tends to a factor exceeding 0.94 of that for the fully periodic case (i.e., 6% smaller). As in the three-dimensional problem, the largest eigenvalue occurs for the spatial frequency $\omega_x h = 2\pi/3$.

2.4   Numerical tests of the scheme

In order to test the implementation of our method we first ran a number of computations without forcing with decreasing grid size h to evaluate the discrete energy C_e as function of time. We took $\mu = 0.16$, $\lambda = 0.49$, $\rho = 1$, and started the computations with the initial data in spherical coordinates:

$$\mathbf{U}_0(r) = \nabla\left(\frac{P_{10}(r)}{r}\right), \quad \mathbf{U}_1(r) = -c_p\nabla\left(\frac{P'_{10}(r)}{r}\right), \quad r = \sqrt{(x-2)^2 + (y-1.5)^2 + (z-1.5)^2}, \tag{69}$$

where $P_{10}(\xi)$ is the four times continously differentiable function

$$P_{10}(\xi) = \begin{cases} 0, & \xi <= 0, \\ 1024\xi^5\left(1 - 5\xi + 10\xi^2 - 10\xi^3 + 5\xi^4 - \xi^5\right), & 0 < \xi < 1, \\ 0, & \xi \geq 1. \end{cases} \tag{70}$$

(We note in passing that $\mathbf{u}(r,t) = \nabla(P_{10}(r - c_p t)/r)$ is an analytic solution of the free space problem.) We impose a stress-free boundary condition at $z = 0$ and enforce zero displacement conditions on all other boundaries. The size of the computational domain was $a = 4$, $b = 3$, and $c = 3$. Since there is no forcing, the discrete energy $C_e(t_n)$ should remain constant. The energy in the continuous problem is often decomposed into its kinematic and potential components,

$$E(t) = K(t) + U(t),$$

where

$$K(t) = \frac{1}{2}\int_\Omega \rho(u_t^2 + v_t^2 + w_t^2)\, d\Omega,$$

$$U(t) = \frac{1}{2}\int_\Omega \lambda(u_x + v_y + w_z)^2 + 2\mu(u_x^2 + v_y^2 + w_z^2) + \mu\left((u_y + v_x)^2 + (u_z + w_x)^2 + (v_z + w_y)^2\right)\, d\Omega.$$

In the absence of forcing, $E(t) = $ const. By dividing (49) by δ_t^2 it is straight forward to see that

$$C_e(t_{n+1}) = 2E(t_{n+1/2}) + \mathcal{O}(h^2).$$

Hence, the discrete energy C_e should not only be conserved in time, but its value should also converge to $2E(t)$ as the grid is refined. Both these properties are confirmed by our calculations, see Figure 3.

As a second test of our implementation, we check the order of accuracy of the scheme using the *method of analytical solutions* (also known as *twilight-zone* forcing [3]). The idea is to construct forcing functions **f** and **g** so that the solution of the test problem becomes a known function $\mathbf{u}^{\mathrm{true}}(\mathbf{x}, t)$. We then solve the test problem using our implementation of the method and compared our numerical results to the known
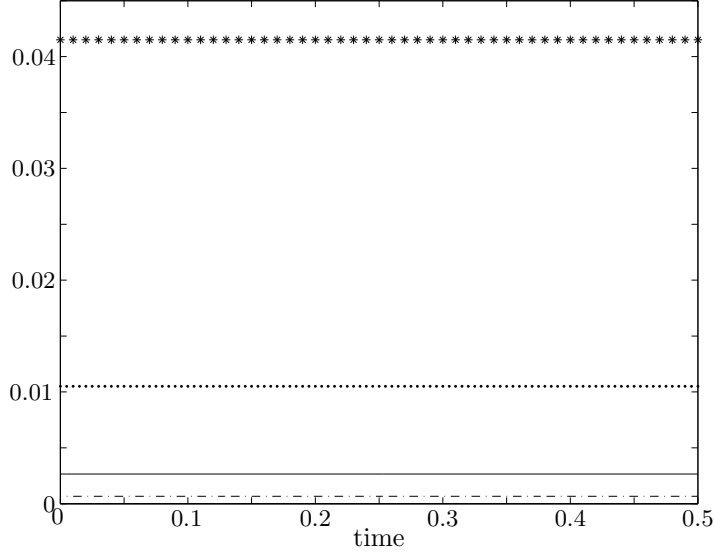
Figure 3: Time evolution of the relative error in the discrete energy $(C_e(t) - 2E(t))/2E(t)$ for different grid sizes. The discrete energy is conserved to within round off errors for all cases. As can be seen the discrete energy converges towards the continuous value at the expected $\mathcal{O}(h^2)$ rate. Here, $h = 0.04\,(*)$, $0.02\,(\cdot)$, $0.01\,(-)$, $0.005\,(-\cdot)$

solution on a succession of finer grids in order to check the convergence properties. Our constructed solution was

$$u^{\text{true}}(\mathbf{x}, t) = \sin(\omega(x - ct))\sin(\omega y)\sin(\omega z),$$
$$v^{\text{true}}(\mathbf{x}, t) = \sin(\omega x)\sin(\omega(y - ct))\sin(\omega z),$$
$$w^{\text{true}}(\mathbf{x}, t) = \sin(\omega x)\sin(\omega y)\sin(\omega(z - ct)),$$

where ω and c are constants. The material properties were chosen to vary smoothly according to

$$\mu(\mathbf{x}) = 1 + \cos^2(\pi x)\cos^2(\pi y)\cos^2(\pi z)$$
$$\lambda(\mathbf{x}) = 1 + \sin^2(\pi x)\sin^2(\pi y)\sin^2(\pi z)$$
$$\rho(\mathbf{x}) = 1.$$

A normal stress condition was imposed on the $z = 0$ surface and inhomogeneous Dirichlet conditions were imposed on all other boundaries. The computational domain had sizes $a = 2$, $b = 2$, and $c = 2$. A number of calculations with increasingly fine grid spacing were run and the errors were evaluated in the discrete max-norm. (The discrete max-norm of a vector grid function $\mathbf{v}_h = (u_h, v_h, w_h)$ is defined as $||\mathbf{v}_h||_\infty = \max(\max_{i,j,k} |u_h|, \max_{i,j,k} |v_h|, \max_{i,j,k} |w_h|)$. As expected we obtained second order convergence when both the forcing and the solution are smooth, see Table 1. Non-smooth forcings and solutions will be discussed in Section 3.

3 Singular source terms

In seismic wave propagation the source term is often applied at a point, along a line, or over a surface in three-dimensional space. Sources along lines or surfaces are commonly decomposed into a number of

18

	$t = 1$	
h	$\lVert \mathbf{v}_h - \mathbf{u}^{\mathrm{true}} \rVert_\infty$	rate
0.04	0.04331	
0.02	0.01062	4.079
0.01	0.002654	4.00
0.005	0.0006627	4.00

Table 1: Errors in max-norm for decreasing h and smooth analytical solution $\mathbf{u}^{\mathrm{true}}$. Convergence rate indicates second order convergence. Here $c = 1$ and $\omega = 2\pi$.

point sources distributed along the corresponding line or surface,

$$\mathbf{f}(\mathbf{x}, t) = \sum_r \mathbf{f}_r^{(F)}(\mathbf{x}, t) + \sum_r \mathbf{f}_r^{(M)}(\mathbf{x}, t). \tag{71}$$

Two types of point sources occur in seismic applications. Point forces ($\mathbf{f}_r^{(F)}$) are, for example, used to model internal forcings due to volcanic eruptions or external forcings applied to the free surface,

$$\mathbf{f}_r^{(F)}(\mathbf{x}, t) = g_r(t)\mathbf{F}_r\delta(\mathbf{x} - \mathbf{x}_r), \tag{72}$$

where $\delta(\mathbf{x})$ is the Dirac distribution and $\mathbf{F}_r$ is a constant vector. The second type of point source is the point moment (or double couple), denoted by $\mathbf{f}_r^{(M)}$ in (71). Point moments are often used to model earthquakes and explosions [2], and are of the form

$$\mathbf{f}_r^{(M)}(\mathbf{x}, t) = g_r(t)\,\mathfrak{M}_r \cdot \nabla\delta(\mathbf{x} - \mathbf{x}_r), \tag{73}$$

where $\nabla\delta(\mathbf{x})$ is the gradient of the Dirac distribution and $\mathfrak{M}_r$ is a constant symmetric tensor.

Each term in (71) is applied at a location (x_r, y_r, z_r) and it is desirable to make this location independent of the grid so that the numerical modeling can be made as accurate as possible and no artifacts are generated by "stair stepping" the point sources along a smooth line or surface in three-dimensional space. Due to the singular nature of point sources, we can only expect the numerical solution to converge away from the location of the sources. Furthermore, we can expect that different numerical techniques are necessary for handling the two types of sources, since the point force depends on the Dirac distribution while the point moment depends on its gradient, which is a more singular function.

The analyses of Waldén [24] and Tornberg and Engquist [22] demonstrate that it is possible to derive regularized approximations of the Dirac distribution and its gradient, which result in point wise convergence of the solution away from the sources. Based on these analyses, we define a hat function,

$$\delta_{\mathrm{hat}}(x) = \frac{1}{h} \begin{cases} 1 - |x|/h, & |x| < h, \\ 0, & \text{elsewhere}, \end{cases} \tag{74}$$

and use $\delta_{\mathrm{hat}}(x - x_r)\delta_{\mathrm{hat}}(y - y_r)\delta_{\mathrm{hat}}(z - z_r)$ to approximate $\delta(\mathbf{x})$ in (72). To approximate the gradient of a Dirac distribution, we start from the piecewise cubic function

$$\delta_{\mathrm{cube}}(x) = \frac{1}{h} \begin{cases} 1 - |x/h|/2 - |x/h|^2 + |x/h|^3/2, & |x| < h, \\ 1 - 11|x/h|/6 + |x/h|^2 - |x/h|^3/6, & h \le |x| < 2h, \\ 0, & \text{elsewhere}. \end{cases} \tag{75}$$

19

We then use

$$
\begin{pmatrix}
\delta'_{\text{cube}}(x - x_r)\delta_{\text{hat}}(y - y_r)\delta_{\text{hat}}(z - z_r) \\
\delta_{\text{hat}}(x - x_r)\delta'_{\text{cube}}(y - y_r)\delta_{\text{hat}}(z - z_r) \\
\delta_{\text{hat}}(x - x_r)\delta_{\text{hat}}(y - y_r)\delta'_{\text{cube}}(z - z_r)
\end{pmatrix}
$$

to approximate the Cartesian components of $\nabla\delta(\mathbf{x} - \mathbf{x}_r)$ in (73). Note that neither (74) nor (75) need to be aligned with the grid.

3.1 Spatial regularity

To study the relation between smoothness of the time function $g(t)$ in the source term, and smoothness in space of the solution, we analyze the related problem of the scalar wave equation with a singular source term. In particular, we study the problem on an infinite domain with the forcing term applied at the point $(0,0,0)$ with homogeneous initial data,

$$
p_{tt} = \nabla^2 p + g(t)\delta(\mathbf{x}), \quad \mathbf{x} \in R^3, \quad t \geq 0,
$$
$$
p(\mathbf{x}, 0) = p_t(\mathbf{x}, 0) = 0,
$$

The Fourier transform of this equation is

$$
\frac{d^2\hat{p}}{dt^2} = -(k_x^2 + k_y^2 + k_z^2)\hat{p} + g(t) \quad t \geq 0, \tag{76}
$$
$$
\hat{p}(k_x, k_y, k_z, 0) = \hat{p}_t(k_x, k_y, k_z, 0) = 0, \tag{77}
$$

where the Fourier transform is given by

$$
\hat{p}(k_x, k_y, k_z, t) = \int \int \int p(x, y, z, t) e^{-i(xk_x + yk_y + zk_z)} \, dx \, dy \, dz.
$$

Equation (76)–(77) is solved by

$$
\hat{p}(k_x, k_y, k_z, t) = \begin{cases} \int_0^t \int_0^\tau g(\tau') \, d\tau' \, d\tau, & k = 0, \\ \frac{1}{k}\left(\sin(kt)\int_0^t \cos(k\tau)g(\tau) \, d\tau - \cos(kt)\int_0^t \sin(k\tau)g(\tau) \, d\tau\right), & k > 0. \end{cases} \tag{78}
$$

where $k = \sqrt{k_x^2 + k_y^2 + k_z^2}$. If $g(t)$ is continuously differentiable, we can integrate (78) by parts,

$$
\hat{p}(k_x, k_y, k_z, t) = \frac{1}{k^2}\left(g(t) - \cos(kt)g(0) - \sin(kt)\int_0^t \sin(k\tau)g'(\tau)d\tau - \cos(kt)\int_0^t \cos(k\tau)g'(\tau)d\tau\right).
$$

By assuming that $g(t)$ has compact support, i.e., $g(t) \equiv 0$ for $t \leq 0$ and $t \geq T$, we get

$$
\hat{p}(k_x, k_y, k_z, t) = \frac{1}{k^2}\left(-\sin(kt)\int_0^t \sin(k\tau)g'(\tau) \, d\tau - \cos(kt)\int_0^t \cos(k\tau)g'(\tau) \, d\tau\right), \quad t \geq T.
$$

The Fourier transform decay as $1/k^2$. We can continue integrating by parts as long as $g(t)$ is sufficiently differentiable, gaining one order of k for each integration. This shows that the solution $p(\mathbf{x}, t)$ has a Fourier transform that decays as $1/k^q$ for $t > T$ if $g(t)$ has compact support and is $q - 1$ times differentiable in time. Furthermore, $\hat{p}$ is bounded because the singularity at $k = 0$ is removable,

$$
\lim_{k \to 0} \hat{p}(k_x, k_y, k_z, t) = \int_0^t (t - \tau)g(\tau) \, d\tau = \int_0^t \int_0^\tau g(\tau') \, d\tau' \, d\tau.
$$

20

Therefore,

$$\int \int \int (1 + k^{2q'}) |\hat{p}|^2 \, dk_x \, dk_y \, dk_z < \infty$$

for $q' < q - 3/2$. By the Sobolev Lemma [8], p can be identified with a function that has m continous derivatives for $m < q' - 3/2 < q - 3$. We conclude that for $t > T$, the solution $p(\mathbf{x}, t)$ will have m continuous derivatives if g is compactly supported and smooth. Here m can be made arbitrarily large by choosing $g(t)$ sufficiently smooth.

If $g(t)$ does not tend to zero for large t, the solution will remain singular at the location of the point source but will be smooth away from it.

3.2 Free space solutions

Let the free space Green's (dyadic) function for the elastic wave equation in a homogeneous material be $\mathfrak{G}(\mathbf{x}, t)$, see [2]. Assuming homogeneous initial data, the analytical solution of the elastic wave equation due to a source function $\mathbf{f}(\mathbf{x}, t)$ follows as the space and time convolution between the Green's function and the source term,

$$\mathbf{u}(\mathbf{x}, t) = \int_t \int_\Omega \mathbf{f}(\mathbf{x}', t') \cdot \mathfrak{G}(\mathbf{x} - \mathbf{x}', t - t') \, d\mathbf{x}' \, dt'.$$

In the special case when the source is a point force, the spatial convolution becomes trivial due to the Dirac distributions in $\mathbf{f}_r^{(F)}$ and the expression reduces to a time integral over t'. Near the source, the solution behaves like $1/|\mathbf{x} - \mathbf{x}_r|$. A closed form solution can be obtained when the time-integration can be performed analytically, for instance when $g(t)$ is a polynomial function.

For a point moment source term $\mathbf{f}_r^{(M)}$, the analytical solution can be written

$$\mathbf{u}(\mathbf{x}, t) = \int_0^t \int_\Omega g_r(t') \left(\mathfrak{M}_r \cdot \nabla \delta(\mathbf{x}' - \mathbf{x}_r) \right) \cdot \mathfrak{G}(\mathbf{x} - \mathbf{x}', t - t') \, d\mathbf{x}' \, dt' = \int_0^t g_r(t') \, \mathfrak{M}_r : \nabla \mathfrak{G}(\mathbf{x} - \mathbf{x}_r, t - t') \, dt',$$

where the colon represents the tensor contraction over two indices. Near the point moment, the solution behaves like $1/|\mathbf{x} - \mathbf{x}_r|^2$, so it is more singular than in the point force case.

To investigate how the numerical solution convergences when the source function is singular, we ran a number of tests with point forces and point moments using the time function $g(t) = P_{10}(t)$ defined in (70). This function has compact support in $0 \le t \le 1$ and is four times continuously differentiable. We took a computational domain with $a = 2$, $b = 2$, $c = 2$, and used the material parameters $\rho = 1$, $\lambda = 0.32$, $\mu = 0.16$. Dirichlet boundary conditions were enforced on all boundaries, but the boundaries have no influence on the solution until $t > 1.25$ since $c_p = 0.8$ and the point sources were centered at $\mathbf{x}_r = (1, 1, 1)$. The errors were measured at two different times in discrete max-, 2- and 1-norms. Since the analytical solution is singular at the point where the source applies, that point was excluded from the calculation of the norms. (The 2- and 1-norms for a vector grid function $\mathbf{u}$ are defined as $||\mathbf{u}||_2^2 = h^3 \sum_{i,j,k} (|u_{i,j,k}|^2 + |v_{i,j,k}|^2 + |w_{i,j,k}|^2)$ and $||\mathbf{u}||_1 = h^3 \sum_{i,j,k} (|u_{i,j,k}| + |v_{i,j,k}| + |w_{i,j,k}|)$.) First we evaluated the errors at $t = 0.5$ when $g(t) > 0$, see Table 2. As expected we did not achieve second order convergence because the solution of the continuous problem is singular. Also note that the convergence rate is slower for the point moment source than in the less singular point force case. In Figure 4, we show the errors as function of the distance from the singularity. Away from the singularity, the errors are smooth in space and decay like $\mathcal{O}(h^2)$ as the grid size tends to zero. However, near the source the errors do not decay as the grid is refined and this explains the convergence numbers in Table 2. Secondly, we evaluated the errors at $t = 1.2$, when $g(t) = 0$, see Table 3. After the source term has vanished the solution becomes smooth everywhere and our results show the proper second order convergence rate in accordance with theory.

	point force					
h	$\frac{\|\|\mathbf{v}_h-\mathbf{u}\|\|_\infty}{\|\|\mathbf{v}_h\|\|_\infty}$	$\frac{\|\|\mathbf{v}_h-\mathbf{u}\|\|_2}{\|\|\mathbf{v}_h\|\|_2}$	$\frac{\|\|\mathbf{v}_h-\mathbf{u}\|\|_1}{\|\|\mathbf{v}_h\|\|_1}$	rate$^\infty$	rate^2	rate^1
0.04	0.04833	0.08293	0.1011			
0.02	0.04108	0.05174	0.03248	1.176	1.602	3.113
0.01	0.03936	0.03525	0.009970	1.043	1.467	3.257
0.005	0.03894	0.02470	0.002955	1.010	1.427	3.373

	point moment					
h	$\frac{\|\|\mathbf{v}_h-\mathbf{u}\|\|_\infty}{\|\|\mathbf{v}_h\|\|_\infty}$	$\frac{\|\|\mathbf{v}_h-\mathbf{u}\|\|_2}{\|\|\mathbf{v}_h\|\|_2}$	$\frac{\|\|\mathbf{v}_h-\mathbf{u}\|\|_1}{\|\|\mathbf{v}_h\|\|_1}$	rate$^\infty$	rate^2	rate^1
0.04	0.3051	0.2805	0.2272			
0.02	0.3208	0.2760	0.1154	0.9509	1.016	1.969
0.01	0.3253	0.2769	0.05759	0.9871	0.9967	2.003
0.005	0.3264	0.2782	0.02872	0.9970	0.9953	2.005

Table 2: Relative error in the numerical solution of the free space problem at time $t = 0.5$ (singular solution) due to a point force (top) and a point moment (bottom), measured in max-, 2- and 1-norms. Here $\mathbf{v}_h$ and $\mathbf{u}$ denote the numerical and analytical solutions, respectively.
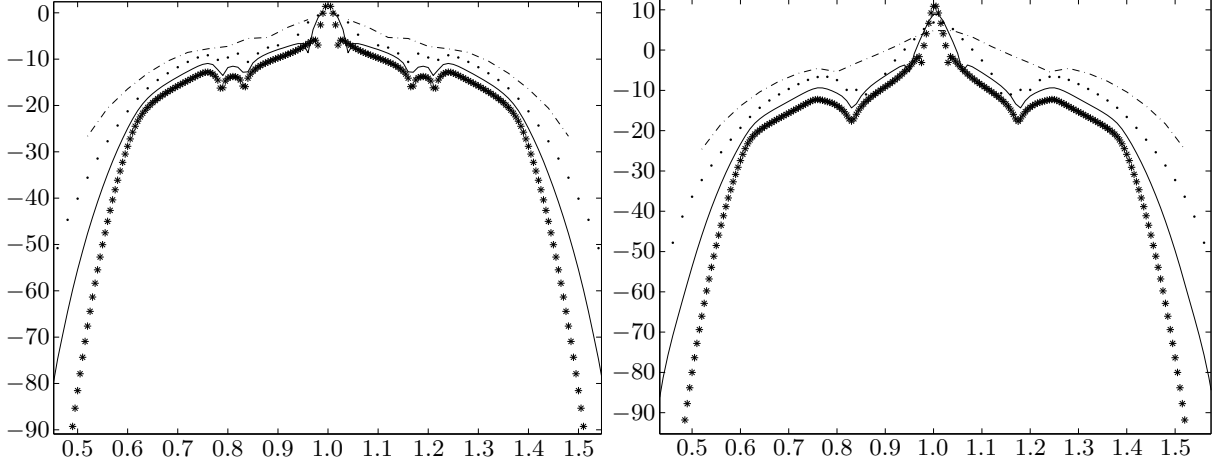
Figure 4: The 2−logarithm of the error along a line going through the source point for a point force (left) and a point moment source (right), both located at $x = 1$. Note that the error decays as $\mathcal{O}(h^2)$ away from the source, but not near it. Near the source, the error is about $2^{11} \approx 2000$ times larger for the point moment than for the point force. The grid sizes were $h = 0.04\,(-\cdot)$, $0.02\,(\cdot)$, $0.01\,(-)$, $0.005\,(\ast)$.

22

	point force					
h	$\frac{\|\|\mathbf{v}_h-\mathbf{u}\|\|_\infty}{\|\|\mathbf{v}_h\|\|_\infty}$	$\frac{\|\|\mathbf{v}_h-\mathbf{u}\|\|_2}{\|\|\mathbf{v}_h\|\|_2}$	$\frac{\|\|\mathbf{v}_h-\mathbf{u}\|\|_1}{\|\|\mathbf{v}_h\|\|_1}$	rate$^\infty$	rate^2	rate^1
0.04	0.04516	0.03984	0.04122			
0.02	0.01180	0.01001	0.01025	3.831	3.984	4.021
0.01	0.003023	0.002512	0.002560	3.907	3.988	4.004
0.005	0.0007592	0.0006287	0.0006400	3.983	4.000	4.00
	point moment					
h	$\frac{\|\|\mathbf{v}_h-\mathbf{u}\|\|_\infty}{\|\|\mathbf{v}_h\|\|_\infty}$	$\frac{\|\|\mathbf{v}_h-\mathbf{u}\|\|_2}{\|\|\mathbf{v}_h\|\|_2}$	$\frac{\|\|\mathbf{v}_h-\mathbf{u}\|\|_1}{\|\|\mathbf{v}_h\|\|_1}$	rate$^\infty$	rate^2	rate^1
0.04	0.1170	0.1016	0.09981			
0.02	0.03400	0.02762	0.02681	3.440	3.678	3.724
0.01	0.008872	0.007109	0.006855	3.833	3.885	3.908
0.005	0.002244	0.001793	0.001724	3.961	3.972	3.985

Table 3: Relative error in the numerical solution of the free space problem at time $t = 1.2$ (smooth solution) due to a point force (top) and a point moment (bottom), measured in max-, 2- and 1-norms. Here $\mathbf{v}_h$ and $\mathbf{u}$ denote the numerical and analytical solutions, respectively.

We remark that in the point moment source case it is important to use the δ'_{cube} approximation in the gradient of the Dirac distribution, as opposed to δ'_{hat}. Otherwise the convergence rate will be slower than second order in the grid size (example not shown to conserve space).

3.3   Half spaces and Lamb's problem

Point forcing on the boundary of a half space is referred to as Lamb's problem [18]. Analytical solutions for the three-dimensional problem have been presented by a number of authors with different degrees of applicability. For the case of a point force directed normal to the free surface $z = 0$, the general solution can be found in [20] or [6]. To test the accuracy of the numerical solutions, we performed a grid refinement study on a computational domain with sizes $a = 4$, $b = 4$, $c = 2$, enforcing a free surface boundary condition along $z = 0$ and Dirichlet conditions on all other boundaries. We assumed a Poisson material with $\rho = 1$, $\mu = 1$, and $\lambda = 1$, i.e., $c_p/c_s = \sqrt{3}$, and used the same time function $g(t)$ as in the free space case. In this experiment, the point force was applied at $\mathbf{x}_r = (2, 2, 0)$, so the Dirichlet boundaries should not effect the solution until $t > 1.15$. The error in the numerical solution was evaluated both at $t = 0.5$, when the solution of the continuous problem is singular, and at $t = 1.1$ when the solution is smooth. We only report the error along the free surface, because the analytical solution is difficult to evaluate in the interior of the domain. As in the free space problem, we observe second order convergence only when the solution is smooth in space, see Table 4.

	$t = 0.5$					
h	$\frac{\|\|\mathbf{v}_h-\mathbf{u}\|\|_\infty}{\|\|\mathbf{v}_h\|\|_\infty}$	$\frac{\|\|\mathbf{v}_h-\mathbf{u}\|\|_2}{\|\|\mathbf{v}_h\|\|_2}$	$\frac{\|\|\mathbf{v}_h-\mathbf{u}\|\|_1}{\|\|\mathbf{v}_h\|\|_1}$	rate$^\infty$	rate^2	rate^1
0.04	0.02797	0.08631	0.2007			
0.02	0.01758	0.05312	0.1102	1.591	1.625	1.821
0.01	0.01547	0.04002	0.05028	1.136	1.327	2.192
0.005	0.01696	0.03696	0.02305	0.9121	1.083	2.181
	$t = 1.1$					
h	$\frac{\|\|\mathbf{v}_h-\mathbf{u}\|\|_\infty}{\|\|\mathbf{v}_h\|\|_\infty}$	$\frac{\|\|\mathbf{v}_h-\mathbf{u}\|\|_2}{\|\|\mathbf{v}_h\|\|_2}$	$\frac{\|\|\mathbf{v}_h-\mathbf{u}\|\|_1}{\|\|\mathbf{v}_h\|\|_1}$	rate$^\infty$	rate^2	rate^1
0.04	0.2892	0.3081	0.3686			
0.02	0.1082	0.1186	0.1408	2.673	2.598	2.618
0.01	0.03138	0.03496	0.04175	3.448	3.392	3.372
0.005	0.008189	0.009194	0.01100	3.832	3.802	3.795

Table 4: Relative error in the numerical solution of Lamb's problem at $t = 0.5$ (top) (when the solution is singular), and at $t = 1.1$ (bottom) (when the solution is smooth), measured in max-, 2- and 1- norms. Here $\mathbf{v}_h$ and $\mathbf{u}$ denote the numerical and analytical solutions, respectively.

4   Applications and extensions of the method

4.1   Surface waves

The elastodynamic equations together with the stress free boundary condition admit solutions in the form of surface waves, i.e., waves propagating along the surface with amplitude decaying exponentially away from the surface. For the homogeneous two-dimensional half plane problem in $z \geq 0$, these solutions are commonly referred to as Rayleigh waves and have the form

$$u(x,z,t) = A\left(e^{-\eta_p\omega z} - \left(1 - \frac{c_r^2}{2c_s^2}\right)e^{-\eta_s\omega z}\right)\sin(\omega(c_r t - x)), \tag{79}$$

$$w(x,z,t) = A\left(1 - \frac{c_r^2}{c_p^2}\right)^{1/2}\left(-e^{-\eta_p\omega z} + \left(1 - \frac{c_r^2}{2c_s^2}\right)^{-1}e^{-\eta_s\omega z}\right)\cos(\omega(c_r t - x)), \tag{80}$$

where

$$\eta_p = \left(1 - \frac{c_r^2}{c_p^2}\right)^{1/2}, \quad \eta_s = \left(1 - \frac{c_r^2}{c_s^2}\right)^{1/2}.$$

Here, c_r is the phase velocity of the wave, which is the real root of the Rayleigh equation

$$\left(2 - \frac{c_r^2}{c_s^2}\right)^2 - 4\left(1 - \frac{c_r^2}{c_p^2}\right)^{1/2}\left(1 - \frac{c_r^2}{c_s^2}\right)^{1/2} = 0, \quad 0 < c_r < c_s.$$

The waves described by (79)-(80) are non-dispersive, i.e. c_r is independent of ω. However, the discretization introduce errors that can be interpreted as a numerical dispersion relation where the phase velocity depends on the resolution on the grid. The numerical dispersion relation for our interior difference stencil coincides with previous central difference schemes which were analyzed by Cohen [5]. For

			c_r^*/c_r	
PPW	$\nu = 2$	$\nu = 3$	$\nu = 5$	$\nu = 10$
40	1.0028	1.0065	1.017	1.055
20	1.011	1.022	1.052	1.12
10	1.031	1.06	1.11	1.2
8	1.043	1.083	1.13	1.5
6	1.049	1.095	1.35	1.63
5	1.07	1.11	1.4	1.72
4	1.095	1.14	1.65	1.78
3.5	1.16	1.4	2.76	2.9

Table 5: Numerical dispersion relation for the finite difference scheme applied to Rayleigh waves. The table shows the ratio between the estimated phase velocity in the numerical solution and its continuous value, for different number of grid points per wave length (PPW) and ν.

surface waves, the numerical dispersion relation provides the numerical phase velocity c_r^* as a function of the resolution ωh, which often is expressed in terms of the number of grid points per wavelength,

$$\mathrm{PPW} = \frac{2\pi}{\omega h}.$$

Since it is very complicated to analytically derive the numerical dispersion relation for surface waves, we instead investigate the relation by numerical experiments using a two-dimensional version of our method. A free surface condition was imposed at $z = 0$ and periodic boundary conditions were used in the x-direction. We enforced (79)-(80) as initial data, which only contains a single spatial frequency ω. Hence, the numerical solution should essentially advect the initial data with a modified phase velocity c_r^*. We determined c_r^* by visually inspecting the solution along the surface at time $t = 1/c_r$, and comparing the positions of the numerical and analytical solutions, see Table 5. Note that the visual inspection is not very precise when the solution is poorly resolved on the grid (PPW < 5), so these results should be interpreted accordingly. Despite this uncertainty, it is clear that the numerical phase velocity increases rapidly as ωh approaches $2\pi/3$ and $\nu \geq 3$. It is interesting to note that this value of ωh coincides with the spatial frequency of the fast surface waves which determine the stability limit of the time step, cf. Section 2.3.

4.2   Non-reflecting boundary conditions

When modeling seismic events such as the simplified earthquake in Section 4.3, it is desirable to truncate the computational domain without causing significant amounts of artificial reflections. Many different methods, including absorbing, non-reflecting, and perfectly matching techniques have been proposed in the literature. Here we will use the first order non-reflecting boundary conditions developed by Clayton and Engquist [4]. The well-known idea behind these boundary conditions is to impose a differential equation on the boundary which allows wave propagation only in the outward direction. For boundaries with $x = const.$, the boundary conditions are

$$u_t = \pm c_p u_x, \; v_t = \pm c_s v_x, \; w_t = \pm c_s w_x, \tag{81}$$

25

where the positive signs are taken for the lower boundary $x = 0$ and the negative signs for the upper boundary $x = a$. Similar advection equations are imposed at boundaries with $y = const.$ or $z = const.$

Away from edges in the computational domain, we have found that the box scheme discretization [4] of the boundary condition (81) works well. At the edges of the domain, i.e., where two non-reflecting boundaries meet, Clayton and Engquist suggested applying the non-reflecting boundary condition in a diagonal direction. However, we have found that imposing compatibility conditions along the edges result in a more rubust method which also is easier to implement. We examplify the compatibility conditions on the edge where $x = 0$ and $y = 0$. Along the boundary $x = 0$, we impose (81) (with the positive sign). The corresponding boundary conditions along $y = 0$ are

$$u_t = c_s u_y, \ v_t = c_p v_y, \ w_t = c_s w_y, \quad y = 0, \ 0 \le x \le a, \ 0 \le z \le c, \ t \ge 0.$$

Equating the time derivatives along the edge gives

$$\begin{aligned} c_p u_x &= c_s u_y, \\ c_s v_x &= c_p v_y, \quad y = 0, \ x = 0, \ 0 \le z \le c, \ t \ge 0, \\ c_s w_x &= c_s w_y. \end{aligned}$$

Similar relations can easily be derived for the other edges.

4.3   A simplified earthquake

The Pacific Earthquake Engineering Center and the Southern California Earthquake Center have defined a set of seismic model problems in an effort to evaluate and validate wave propagation software [7]. We have computed solutions to several of these problems but in order to save space we only report our results for problem LOH.2, which models a simplified earthquake with slip on an extended fault surface, see Figure 5. The material in this model consists of a layer over a half-space, where the layer extends from depth $z = 0$ to $z = 1000$. The velocities and density in the layer are $c_p = 4000$, $c_s = 2000$, $\rho = 2600$. The half-space $z \ge 1000$ has the material properties $c_p = 6000$, $c_s = 3464$, $\rho = 2700$.

The slip on the extended fault is modeled by distributing point moment sources on a regular grid with size δ_s (which is independent of the grid size h) over the fault surface $x = 0$, $0 \le y \le 8000$, $2000 \le z \le 6000$. In this case, the fault slips by a constant amount in the y-direction, which means that the Cartesian components of the moment tensor $\mathfrak{M}_r$ in each source term (73) equals

$$\mathfrak{M}_r = \delta_s^2 \mu S_0 \begin{pmatrix} 0 & 1 & 0 \\ 1 & 0 & 0 \\ 0 & 0 & 0 \end{pmatrix}, \quad S_0 = 1.$$

The modeled earthquake starts at the hypocenter $\mathbf{x}_H = (0, 1000, 4000)$, and the rupture propagates along the fault surface with a uniform rupture velocity of 3000. The propagation of the rupture is modeled by letting the source time function $g_r(t)$ depend on the distance between the hypocenter and the location of each source,

$$R_r = |\mathbf{x}_r - \mathbf{x}_H|.$$

The time dependence of source number r is

$$g_r(t) = \begin{cases} 0, & t < R_r/3000, \\ 1 - \left(1 + \dfrac{\tau_r(t)}{T}\right) e^{-\tau_r(t)/T}, & t \ge R_r/3000, \end{cases} \quad \tau_r(t) = t - R_r/3000,$$
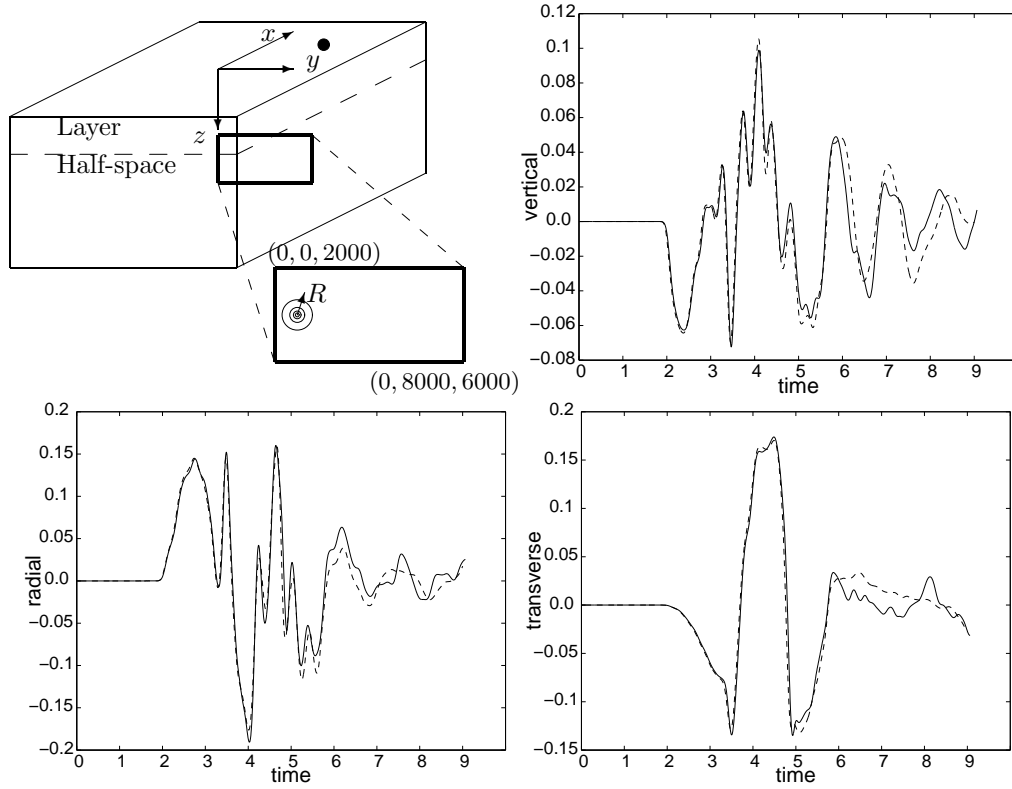
Figure 5: The computational domain and fault surface for the simplified earthquake problem LOH.2 (upper left). The • indicates the measurement station and the magnified plane shows the fault surface, where the slip starts at the hypocenter indicated by concentric circles. Our results are shown with solid lines for the vertical (top right), radial (bottom left), and transverse (bottom right) velocity components, and the dashed lines are the results from the UCSB code, see [7].

where $T = 0.1$ is related to the rise-time of the slip, i.e., how quickly the fault slips at each fixed point along the fault surface.

In our calculation, the extent of the computational domain was $-15,000 \leq x \leq 15,000$, $-15,000 \leq y \leq 15,000$, $0 \leq z \leq 17,000$, and non-reflecting boundary conditions were imposed on all boundaries except at $z = 0$, where a free surface condition was enforced. The grid size was $h = 50$ corresponding to about 1.23×10^8 grid points, and 1,742 time steps were taken to reach time $t = 9$. We discretized the fault surface with $\delta_s = 100$, giving 3200 point moment sources. Results for this problem are available from a number of finite-difference and finite-element codes [7]. To compare our results, we recorded the time evolution of the velocity (i.e., the time derivative of the displacement) at a number of stations along a line on the free surface. Since all codes predicted similar results, we only show the comparison with the UCSB code (using notation from [7]). This code solves the elastic wave equation as a first order system in velocity-stress formulation using a staggered grid finite-difference method. Since the source time functions $g_r(t)$ trigger high frequency motions which are not resolvable on the mesh, the results from both our and the UCSB code were low-pass filtered in time using a Gaussian with filter width $\sigma = 0.05$. In Figure 5 we compare solutions at a station located at $\mathbf{x} = (6000, 8000, 0)$. Velocities are given in a cylindrical coordinate system (radial, transverse, up) with origin at $(0, 0, 0)$. Note that the non-reflecting boundary conditions only effect the solution after $t \approx 5$ and that our results compare especially well with

the other code before that time. One way of determining the accuracy of the solution after $t \approx 5$ would be to repeat the simulation on a larger domain, but the computational cost was too great to perform that experiment.

5 Conclusions

We have described a stable, second order accurate finite difference method for the elastic wave equation in second order formulation subject to a stress-free boundary condition on a flat surface. We have proven that the method is stable even when the coefficients are discontinuous in space, as long as $\mu > 0$, $\lambda > 0$, and $\rho > 0$ at all grid points. The stability limit on the time step has been studied in detail, and we have shown that all values of $c_p/c_s > \sqrt{2}$ can be handled if the time step is reduced by 9% compared to the von Neumann value. We have also described a way to discretize point forces and moments on the mesh so that the solution becomes second order accurate away from the singularity in the solution.

In seismic applications it is common to have water (e.g., a lake or an ocean) in parts of the domain. Only compressional (P-) waves can travel through water and the acoustic wave propagation can be modeled by setting $\mu = 0$ in the elastic wave equation. We have generalized our scheme to handle the mixed elastic/acoustic case, and this scheme was used as part of a simulation effort coordinated by the U.S. Geological Survey to model ground motions during the great 1906 San Francisco earthquake [21]. Our results showed good agreement with other codes and measured Mercalli intensities. More details will be described in a forthcoming paper.

Future plans include generalizing our embedded boundary technique for the scalar wave equation [17, 15, 14], to the elastic wave equation. In the seismic application, embedded boundaries will allow us to include effects of topography and more accurately treat internal material discontinuities.

Acknowledgments

A Accuracy (Theorem 1)

We will prove the accuracy of the semi-discrete equations by showing that they are equivalent to another approximation which clearly is second order accurate. In particular, we want to analyze the accuracy of the spatial discretization (17), (18), (19) at the $z = 0$ boundary, where the free surface boundary condition is applied. At this boundary, the operator $\widetilde{D_0^z}$ simplifies to D_+^z, which would appear to only give a first order accurate difference formula. However, we proceed to show that this difference formula, in combination with the discrete free-surface boundary condition, indeed results in a second order approximation.

We start by eliminating the ghost points above the free surface from the semi-discrete system (17), (18), (19), subject to the boundary conditions (20), (21), and (22). To save space, we only go through the details for (17) subject to (20). The terms in $L^{(u)}$ that contain z-differences on the $z = 0$ grid line are

$$T_{i,j} =: D_-^z \left(\mu_{i,j,3/2} D_+^z u_{i,j,1} \right) + D_0^x \left(\lambda_{i,j,1} D_+^z w_{i,j,1} \right) + D_+^z \left(\mu_{i,j,1} D_0^x w_{i,j,1} \right),$$

The free surface boundary condition (20) gives

$$\mu_{i,j,1/2} D_+^z u_{i,j,0} = -\mu_{i,j,3/2} D_+^z u_{i,j,1} - 2\mu_{i,j,1} D_0^x w_{i,j,1}.$$

28

Hence,

$$T_{i,j} = \frac{2}{h} \left[\mu_{i,j,3/2} D_+^z u_{i,j,1} + \mu_{i,j,1} D_0^x w_{i,j,1} \right] + D_0^x \left(\lambda_{i,j,1} D_+^z w_{i,j,1} \right) + D_+^z \left(\mu_{i,j,1} D_0^x w_{i,j,1} \right). \qquad (82)$$

We compare the spatial discretization to a fully centered scheme where the terms in $L^{(u)}$ that contain z-differences on the $z = 0$ grid line,

$$\widetilde{T}_{i,j} =: D_-^z \left(\mu_{i,j,3/2} D_+^z u_{i,j,1} \right) + D_0^x \left(\lambda_{i,j,1} D_0^z w_{i,j,1} \right) + D_0^z \left(\mu_{i,j,1} D_0^x w_{i,j,1} \right). \qquad (83)$$

We can perturb the free surface boundary condition (20) by a second order term,

$$\frac{1}{2} \left(\mu_{i,j,3/2} D_+^z u_{i,j,1} + \mu_{i,j,1/2} D_+^z u_{i,j,0} \right) + \mu_{i,j,1} D_0^x w_{i,j,1} = h^2 R_{i,j}. \qquad (84)$$

The resulting spatial discretization will be second order accurate as long as R is a difference operator which is bounded independently of h for smooth functions. We will determine R such that (83) subject to (84) is equivalent to (82). The boundary condition (84) gives

$$\mu_{i,j,1/2} D_+^z u_{i,j,0} = -\mu_{i,j,3/2} D_+^z u_{i,j,1} - 2\mu_{i,j,1} D_0^x w_{i,j,1} + 2h^2 R_{i,j}. \qquad (85)$$

Using (85), (83) can be written

$$\widetilde{T}_{i,j} = \frac{2}{h} \left[\mu_{i,j,3/2} D_+^z u_{i,j,1} + \mu_{i,j,1} D_0^x w_{i,j,1} \right] + D_0^x \left(\lambda_{i,j,1} D_0^z w_{i,j,1} \right) + D_0^z \left(\mu_{i,j,1} D_0^x w_{i,j,1} \right) + 2h R_{i,j}.$$

Hence, $T = \widetilde{T}$ if

$$D_0^x \left(\lambda_{i,j,1} D_+^z w_{i,j,1} \right) + D_+^z \left(\mu_{i,j,1} D_0^x w_{i,j,1} \right) = D_0^x \left(\lambda_{i,j,1} D_0^z w_{i,j,1} \right) + D_0^z \left(\mu_{i,j,1} D_0^x w_{i,j,1} \right) + 2h R_{i,j}.$$

We have

$$D_0^z w = D_+^z w - \frac{h}{2} D_+^z D_-^z w,$$

which gives

$$R_{i,j} = \frac{1}{4} D_0^x (\lambda_{i,j,1} D_+^z D_-^z w_{i,j,1}) + \frac{1}{4} D_+^z D_-^z (\mu_{i,j,1} D_0^x w_{i,j,1}).$$

Similar calculations show that the boundary conditions (21) and (22) can be perturbed by second order terms to account for the difference between a fully centered and a one-sided spatial discretization in $L^{(v)}$ and $L^{(w)}$, respectively.

This proves that the semi-discrete approximation (17)-(19) subject to the boundary conditions (20)-(22) is second order accurate. $\square$

Note: Inserting the expression for $R_{i,j}$ into (84) shows that the fully centered approximation couples all ghost points $(k = 0)$ along the free surface. Hence, using this formulation would require a linear system to be solved to obtain the ghost point values at each time step. As we have demonstrated, the same solution can be obtained without solving a linear system by using our one-sided formula on the boundary.

B   Self-adjointness of the spatial operator (Lemma 1)

It is straight forward to show the following summation by parts identities:

$$(w, D^z_- v)_h = -(D^z_+ w, v)_h - \frac{h^2}{2} \sum_{i,j} (w_{i,j,2} v_{i,j,1} + w_{i,j,1} v_{i,j,0}) + h^2 \sum_{i,j} w_{i,j,N_z} v_{i,j,N_z-1}, \tag{86}$$

$$(w, \widetilde{D^z_0} v)_h = -(\widetilde{D^z_0} w, v)_h - h^2 \sum_{i,j} w_{i,j,1} v_{i,j,1} + \frac{h^2}{2} \sum_{i,j} (w_{i,j,N_z-1} v_{i,j,N_z} + w_{i,j,N_z} v_{i,j,N_z-1}), \tag{87}$$

where $\sum_{i,j} = \sum_{i=1}^{N_x-1} \sum_{j=1}^{N_y-1}$. Since the solution satisfies periodic boundary conditions in the x and y-directions, we have

$$(w, D^x_- v)_h = -(D^x_+ w, v)_h, \quad (w, D^x_0 v)_h = -(D^x_0 w, v)_h, \tag{88}$$

$$(w, D^y_- v)_h = -(D^y_+ w, v)_h, \quad (w, D^y_0 v)_h = -(D^y_0 w, v)_h. \tag{89}$$

Consider the three terms in the left hand side of (26): $LHS := I + II + III$,

$$I = \left(u^0, L^{(u)}(u^1, v^1, w^1)\right)_h, \quad II = \left(v^0, L^{(v)}(u^1, v^1, w^1)\right)_h, \quad III = \left(w^0, L^{(w)}(u^1, v^1, w^1)\right)_h.$$

Applying the summation by parts identities (86)-(89) on the first term gives

$$I = -\left(D^x_+ u^0, E^x_{1/2}(2\mu+\lambda) D^x_+ u^1\right)_h - \left(D^y_+ u^0, E^y_{1/2}(\mu) D^y_+ u^1\right)_h - \left(D^z_+ u^0, E^z_{1/2}(\mu) D^z_+ u^1\right)_h$$
$$- \left(D^x_0 u^0, \lambda D^y_0 v^1 + \lambda \widetilde{D^z_0} w^1\right)_h - \left(D^y_0 u^0, \mu D^x_0 v^1\right)_h - \left(\widetilde{D^z_0} u^0, \mu D^x_0 w^1\right)_h + B^{(u)}, \tag{90}$$

where the boundary terms are

$$B^{(u)} = -\frac{h^2}{2} \sum_{i,j} \left(u^0_{i,j,2} \mu_{i,j,3/2} D^z_+ u^1_{i,j,1} + u^0_{i,j,1} \mu_{i,j,1/2} D^z_+ u^1_{i,j,0}\right)$$
$$- h^2 \sum_{i,j} u^0_{i,j,1} \mu_{i,j,1} D^x_0 w^1_{i,j,1} + h^2 \sum_{i,j} u^0_{i,j,N_z} \mu_{i,j,N_z-1/2} D^z_+ u^1_{i,j,N_z-1}$$
$$+ \frac{h^2}{2} \sum_{i,j} \left(u^0_{i,j,N_z-1} \mu_{i,j,N_z} D^x_0 w^1_{i,j,N_z} + u^0_{i,j,N_z} \mu_{i,j,N_z-1} D^x_0 w^1_{i,j,N_z-1}\right).$$

The homogeneous Dirichlet boundary condition (23) gives

$$u^0_{i,j,N_z} = 0, \quad D^x_0 w^1_{i,j,N_z} = 0.$$

Hence, the third and fourth terms in $B^{(u)}$ vanish. To analyze the first term, we note that

$$u^0_{i,j,2} = u^0_{i,j,1} + h D^z_+ u^0_{i,j,1}.$$

Therefore,

$$B^{(u)} = -\frac{h^2}{2} \sum_{i,j} u^0_{i,j,1} \left(\mu_{i,j,3/2} D^z_+ u^1_{i,j,1} + \mu_{i,j,1/2} D^z_+ u^1_{i,j,0} + 2\mu_{i,j,1} D^x_0 w^1_{i,j,1}\right)$$
$$- \frac{h^3}{2} \sum_{i,j} \mu_{i,j,3/2} D^z_+ u^0_{i,j,1} D^z_+ u^1_{i,j,1}. \tag{91}$$

The first term in (91) vanishes because of the free-surface boundary condition (20) and we arrive at

$$B^{(u)} = -\frac{h^3}{2} \sum_{i,j} \mu_{i,j,3/2} D_+^z u_{i,j,1}^0 D_+^z u_{i,j,1}^1.$$

The second term in LHS can be analyzed in the same way giving

$$II = - \left(D_+^x v^0, E_{1/2}^x(\mu) D_+^x v^1 \right)_h - \left(D_+^y v^0, E_{1/2}^y(2\mu + \lambda) D_+^y v^1 \right)_h - \left(D_+^z v^0, E_{1/2}^z(\mu) D_+^z v^1 \right)_h$$
$$- \left(D_0^x v^0, \mu D_0^y u^1 \right)_h - \left(D_0^y v^0, \lambda D_0^x u^1 + \lambda \widetilde{D_0^z} w^1 \right)_h - \left(\widetilde{D_0^z} v^0, \mu D_0^y w^1 \right)_h + B^{(v)}, \quad (92)$$

where

$$B^{(v)} = -\frac{h^3}{2} \sum_{i,j} \mu_{i,j,3/2} D_+^z v_{i,j,1}^0 D_+^z v_{i,j,1}^1.$$

For the third term in LHS we get

$$III = - \left(D_+^x w^0, E_{1/2}^x(\mu) D_+^x w^1 \right)_h - \left(D_+^y w^0, E_{1/2}^y(\mu) D_+^y w^1 \right)_h - \left(D_+^z w^0, E_{1/2}^z(2\mu + \lambda) D_+^z w^1 \right)_h$$
$$- \left(D_0^x w^0, \mu \widetilde{D_0^z} u^1 \right)_h - \left(D_0^y w^0, \mu \widetilde{D_0^z} v^1 \right)_h - \left(\widetilde{D_0^z} w^0, \lambda D_0^x u^1 + \lambda D_0^y v^1 \right)_h + B^{(w)}, \quad (93)$$

where

$$B^{(w)} = -\frac{h^3}{2} \sum_{i,j} (2\mu_{i,j,3/2} + \lambda_{i,j,3/2}) D_+^z w_{i,j,1}^0 D_+^z w_{i,j,1}^1.$$

After applying the same summation by parts rules to the right hand side of (26) it is straight forward to verify that the right hand side equals the left hand side. □

C Ellipticity of the spatial operator (Lemma 3)

We will mimic the construction of the energy in the continuous case by exploring the identity

$$D_-^x E_{1/2}^x(\mu) D_+^x u = D_0^x (\mu D_0^x u) - \frac{h^2}{4} D_+^x D_-^x (\mu D_+^x D_-^x u) \qquad (94)$$

in the periodic x- and y-directions. The problem is not periodic in the z-direction. We will use the following summation-by-parts form of the above identity instead ($N = N_z$ in this appendix)

$$\left(u, D_-^z E_{1/2}^z(\mu) D_+^z u \right)_h = - \left(\widetilde{D_0^z} u, \mu \widetilde{D_0^z} u \right)_h - \frac{h^2}{4} \left(D_+^z D_-^z u, \mu D_+^z D_-^z u \right)_{hr}$$
$$+ h^2 \sum_{i,j} (-\frac{1}{2} \mu_{i,j,1/2} u_{i,j,1} D_+^z u_{i,j,0} - \frac{1}{2} \mu_{i,j,3/2} u_{i,j,1} D_+^z u_{i,j,1}$$
$$+ \frac{\mu_{i,j,N}}{2} u_{i,j,N-1} D_+^z u_{i,j,N-1} + \frac{\mu_{i,j,N-1}}{2} u_{i,j,N} D_+^z u_{i,j,N-1}) \quad (95)$$

We obtain, by use of (94) in the periodic directions,

$$L^{(u)}(u, v, w) = 2D_-^x \left(E_{1/2}^x(\mu) D_+^x u \right) + D_-^z \left(E_{1/2}^z(\mu) D_+^z u \right)$$
$$+ D_0^x \left(\lambda(D_0^x u + D_0^y v + \widetilde{D_0^z} w) \right) + D_0^y \left(\mu(D_0^y u + D_0^x v) \right) + \widetilde{D_0^z} \left(\mu D_0^x w \right)$$
$$- \frac{h^2}{4} \left(D_+^x D_-^x (\lambda D_+^x D_-^x u) + D_+^y D_-^y (\mu D_+^y D_-^y u) \right),$$

31

$$L^{(v)}(u,v,w) = 2D_-^y\left(E_{1/2}^y(\mu)D_+^y v\right) + D_-^z\left(E_{1/2}^z(\mu)D_+^z v\right)$$
$$+ D_0^y\left(\lambda(D_0^x u + D_0^y v + \widetilde{D_0^z}w)\right) + D_0^x\left(\mu(D_0^y u + D_0^x v)\right) + \widetilde{D_0^z}\left(\mu D_0^y w\right)$$
$$-\frac{h^2}{4}\left(D_+^x D_-^x(\mu D_+^x D_-^x v) + D_+^y D_-^y(\lambda D_+^y D_-^y v)\right),$$

$$L^{(w)}(u,v,w) = 2D_-^z\left(E_{1/2}^z(\mu)D_+^z w\right) + D_-^z\left(E_{1/2}^z(\lambda)D_+^z w\right)$$
$$+ \widetilde{D_0^z}\left(\lambda(D_0^x u + D_0^y v)\right) + D_0^x\left(\mu(\widetilde{D_0^z}u + D_0^x w)\right) + D_0^y\left(\mu(\widetilde{D_0^z}v + D_0^y w)\right)$$
$$-\frac{h^2}{4}\left(D_+^x D_-^x(\mu D_+^x D_-^x w) + D_+^y D_-^y(\mu D_+^y D_-^y w)\right),$$

Identities (95) and (87) give

$$(u, L^{(u)})_h = -2(D_+^x u, E_{1/2}^x(\mu)D_+^x u)_h - (\widetilde{D_0^z}u, \mu\widetilde{D_0^z}u)_h - \left(D_0^x u, \lambda(D_0^x u + D_0^y v + \widetilde{D_0^z}w)\right)_h$$
$$- (D_0^y u, \mu(D_0^y u + D_0^x v))_h - \left(\widetilde{D_0^z}u, \mu D_0^x w\right)_h$$
$$-\frac{h^2}{4}\left[(D_+^x D_-^x u, \lambda D_+^x D_-^x u)_h + (D_+^y D_-^y u, \mu D_+^y D_-^y u)_h + (D_+^z D_-^z u, \mu D_+^z D_-^z u)_{hr}\right]$$
$$+ T_1^{(u)} + T_N^{(u)}$$

where $T_1^{(u)}$ and $T_N^{(u)}$ are the boundary terms that correspond to the boundary at $k=1$ and at $k=N$, respectively. The periodic directions do not contribute with any boundary terms as seen from (88) and (89). We have

$$T_1^{(u)} = h^2 \sum_{i,j}\left(-\frac{1}{2}\mu_{i,j,1/2}u_{i,j,1}D_+^z u_{i,j,0} - \frac{1}{2}\mu_{i,j,3/2}u_{i,j,1}D_+^z u_{i,j,1} - u_{i,j,1}\mu_{i,j,1}D_0^x w_{i,j,1}\right)$$
$$= h^2 \sum_{i,j}u_{i,j,1}\left(-\frac{1}{2}\mu_{i,j,1/2}D_+^z u_{i,j,0} - \frac{1}{2}\mu_{i,j,3/2}D_+^z u_{i,j,1} - \mu_{i,j,1}D_0^x w_{i,j,1}\right).$$

It follows directly from the free surface boundary condition (20) that $T_1^{(u)} = 0$. The boundary terms at $k=N$ are given by

$$T_N^{(u)} = h^2 \sum_{i,j}(\frac{\mu_{i,j,N-1}}{2}u_{i,j,N}D_0^x w_{i,j,N-1} + \frac{\mu_{i,j,N}u_{i,j,N-1}}{2}D_0^x w_{i,j,N}$$
$$+ \frac{\mu_{i,j,N}}{2}u_{i,j,N-1}D_-^z u_{i,j,N} + \frac{\mu_{i,j,N-1}}{2}u_{i,j,N}D_-^z u_{i,j,N}).$$

The Dirichlet boundary condition at $k=N$ gives

$$T_N^{(u)} = -h\sum_{i,j}\frac{\mu_{i,j,N}}{2}u_{i,j,N-1}^2.$$

Similarly, we obtain

$$(v, L^{(v)})_h = -2(D_+^y v, E_{1/2}^y(\mu) D_+^y v)_h - (\widetilde{D_0^z} v, \mu \widetilde{D_0^z} v)_h - \left(D_0^y v, \lambda(D_0^x u + D_0^y v + \widetilde{D_0^z} w)\right)_h$$

$$- (D_0^x v, \mu(D_0^y u + D_0^x w))_h - \left(\widetilde{D_0^z} v, \mu D_0^y w\right)_h$$

$$- \frac{h^2}{4} \left[(D_+^x D_-^x v, \mu D_+^x D_-^x v)_h + (D_+^y D_-^y v, \lambda D_+^y D_-^y v)_h + (D_+^z D_-^z v, \mu D_+^z D_-^z v)_{hr} \right]$$

$$- h \sum_{i,j} \frac{\mu_{i,j,N}}{2} v_{i,j,N-1}^2.$$

In the z-direction, we make use of (87) and (95) as well as

$$\left(w, D_+^z \left(E_{1/2}^z(\mu) D_-^z w\right)\right)_h = - \left(D_+^z w, E_{1/2}^z(\mu) D_+^z w\right)_h$$

$$+ h^2 \sum_{i,j} -\frac{1}{2} \mu_{i,j,1/2} w_{i,j,1} D_+^z w_{i,j,0} - \frac{1}{2} \mu_{i,j,3/2} w_{i,j,1} D_+^z w_{i,j,1} - \frac{h}{2} \mu_{i,j,3/2} (D_+^z w_{i,j,1})^2$$

$$+ \mu_{i,j,N-1/2} w_{i,j,N} D_+^z w_{i,j,N-1}.$$

We have

$$(w, L^{(w)})_h = -2(D_+^z w, E_{1/2}^z(\mu) D_+^z w)_h - (\widetilde{D_0^z} w, \lambda \widetilde{D_0^z} w)_h - (\widetilde{D_0^z} w, \lambda(D_0^x u + D_0^y v))_h$$

$$- (D_0^x w, \mu(D_0^x w + \widetilde{D_0^z} u))_h - (D_0^y w, \mu(D_0^y w + \widetilde{D_0^z} v))_h$$

$$- \frac{h^2}{4} \left[(D_+^x D_-^x w, \mu D_+^x D_-^x w)_h + (D_+^y D_-^y w, \mu D_+^y D_-^y w)_h + (D_+^z D_-^z w, \lambda D_+^z D_-^z w)_{hr} \right]$$

$$+ T_1^{(w)} + T_N^{(w)},$$

where $T_1^{(w)}$ are the boundary terms that belong to the free surface boundary, and $T_N^{(w)}$ are the boundary terms that belong to the Dirichlet boundary. We have

$$T_1^{(w)} = h^2 \sum_{i,j} -\frac{1}{2} \lambda_{i,j,1/2} w_{i,j,1} D_+^z w_{i,j,0} - \frac{1}{2} \lambda_{i,j,3/2} w_{i,j,1} D_+^z w_{i,j,1} - w_{i,j,1} \lambda_{i,j,1}(D_0^x u_{i,j,1} + D_0^y v_{i,j,1})$$

$$- \mu_{i,j,1/2} w_{i,j,1} D_+^z w_{i,j,0} - \mu_{i,j,3/2} w_{i,j,1} D_+^z w_{i,j,1} - h \mu_{i,j,3/2} (D_+^z w_{i,j,1})^2 =$$

$$h^2 \sum_{i,j} w_{i,j,1}(-\frac{1}{2} \lambda_{i,j,1/2} D_+^z w_{i,j,0} - \frac{1}{2} \lambda_{i,j,3/2} D_+^z w_{i,j,1} - \lambda_{i,j,1}(D_0^x u_{i,j,1} + D_0^y v_{i,j,1})$$

$$- \mu_{i,j,1/2} D_+^z w_{i,j,0} - \mu_{i,j,3/2} D_+^z w_{i,j,1}) - h \mu_{i,j,3/2} (D_+^z w_{i,j,1})^2.$$

The free surface boundary condition (22) gives

$$T_1^{(w)} = -h^3 \sum_{i,j} \mu_{i,j,3/2} (D_+^z w_{i,j,1})^2.$$

At the Dirichlet boundary we have

$$T_N^{(w)} = h^2 \sum_{i,j} 2\mu_{i,j,N-1/2} w_{i,j,N} D_+^z w_{i,j,N-1} + \frac{1}{2} w_{i,j,N-1} \lambda_{i,j,N}(D_0^x u_{i,j,N} + D_0^y v_{i,j,N})$$

$$+ \frac{1}{2} w_{i,j,N} \lambda_{i,j,N-1}(D_0^x u_{i,j,N-1} + D_0^y v_{i,j,N-1}) + \frac{\lambda_{i,j,N}}{2} w_{i,j,N-1} D_+^z w_{i,j,N-1}$$

$$+ \frac{\lambda_{i,j,N-1}}{2} w_{i,j,N} D_+^z w_{i,j,N-1} = -h \sum_{i,j} \frac{\lambda_{i,j,N}}{2} w_{i,j,N-1}^2.$$

Adding the expressions for $(u, L^{(u)})$, $(v, L^{(v)})$, and $(w, L^{(w)})$ results in (28), (29), and (30).

References

[1] Z. S. Alterman and A. Rotenberg. Seismic waves in a quarter plane. *Bulletin of the Seismological Society of America*, 59, 1969.

[2] Ari Ben-Menahem and Sarva Jit Singh. *Seismic Waves and Sources*. Dover Publications, 2000.

[3] G. Chesshire and W. Henshaw. Composite overlapping meshes for the solution of partial differential equations. *Journal of Computational Physics*, 90, 1990.

[4] Robert Clayton and Björn Engquist. Absorbing boundary conditions for acoustic and elastic wave equations. *Bulletin of the Seismological Society of America*, 67, 1977.

[5] Gary C. Cohen. *Higher-Order Numerical Methods for Transient Wave Equations*. Springer, 2002.

[6] A. Cemal Eringen and Erdoğan S. Şuhubi. *Elastodynamics, Volume II*. Elsevier, 1975.

[7] Steven M. Day et al. Test of 3D elastodynamic codes: Final report for lifelines project 1A01. Technical report, Pacific Earthquake Engineering Center, 2001.

[8] G. B. Folland. *Introduction to partial differential equations*. Princeton University Press, 1976.

[9] B. Gustafsson, H.-O. Kreiss, and J. Oliger. *Time dependent problems and difference methods*. Wiley–Interscience, 1995.

[10] B. Gustafsson, H.-O. Kreiss, and A. Sundström. Stability theory of difference approximations for mixed initial boundary value problems. II. *Mathematics of Computation*, 26(119):649–686, 1972.

[11] A. Ilan and D. Loewenthal. Instability of finite difference schemes due to boundary conditions in elastic media. *Geophysical Prospecting*, 24, 1976.

[12] Almoga Ilan. Stability of finite difference schemes for the problem of elastic wave propagation in a quarter plane. *Journal of Computational Physics*, 29, 1978.

[13] Dimitri Komatitsch and Jeroen Tromp. Introduction to the spectral element method for three-dimensional seismic wave propagation. *Geophysical Journal International*, 139, 1999.

[14] Heinz-Otto Kreiss and N. Anders Petersson. An embedded boundary method for the wave equation with discontinuous coefficients. Technical report, UCRL-JRNL-215702, 2005. (accepted for publication in SIAM J. Sci. Comput.).

[15] Heinz-Otto Kreiss and N. Anders Petersson. A second order accurate embedded boundary method for the wave equation with Dirichlet data. *SIAM J. Sci. Comput.*, 27:1141–1167, 2006.

[16] Heinz-Otto Kreiss, N. Anders Petersson, and Jacob Yström. Difference approximations for the second order wave equation. *SIAM Journal on Numerical Analysis*, 40, 2002.

[17] Heinz-Otto Kreiss, N. Anders Petersson, and Jacob Yström. Difference approximations of the Neumann problem for the second order wave equation. *SIAM Journal on Numerical Analysis*, 42, 2004.

[18] Horace Lamb. On the propagation of tremors over the surface of an elastic solid. *Phil. Trans. Roy. Soc. London, Ser. A*, 203, 1904.

[19] R. Madariaga. Dynamics of an expanding circular fault. *Bulletin of the Seismological Society of America*, 66, 1976.

[20] Harold M. Mooney. Some numerical solutions for Lamb's problem. *Bulletin of the Seismological Society of America*, 64, 1974.

[21] N. Anders Petersson, Arthur Rodgers, Mark Duchaineau, Stefan Nilsson, Björn Sjögreen, and Kathleen McCandless. Large scale seismic modeling and visualization of the 1906 San Francisco earthquake. 100th Anniversary Earthquake Conference, Seismological Society of America, April 2006. Also available as Lawrence Livermore National Laboratory report UCRL-ABS-218213.

[22] Anna-Karin Tornberg and Björn Engquist. Numerical approximation of singular source terms in differential equations. *Journal of Computational Physics*, 200, 2004.

[23] John E. Vidale and Robert W. Clayton. A stable free-surface boundary condition for two-dimensional elastic finite-difference wave simulation. *Geophysics*, 51, 1986.

[24] Johan Waldén. On the approximation of singular source terms in differential equations. *Numerical Methods for Partial Differential Equations*, 15, 1999.

University of California
Lawrence Livermore National Laboratory
Technical Information Department
Livermore, CA 94551